Journal of Materials Chemistry A

Silicon Oxycarbide Ceramics as Next Generation Anode Materials for Lithium-Ion Batteries

Journal:	*Journal of Materials Chemistry A*
Manuscript ID	TA-REV-03-2023-001366.R2
Article Type:	Review Article
Date Submitted by the Author:	25-Jun-2023
Complete List of Authors:	Sujith, Ravindran; Birla Institute of Technology and Science - Hyderabad Campus , Mechanical Engineering; Birla Institute of Technology and Science - Hyderabad Campus, Mechanical Engineering Jella, Gangadhar; BITS Pilani - Hyderabad Campus, Mechanical Engineering Greenough, Michelle ; Clemson University Bordia, Rajendra; Clemson University, Department of Materials Science and Engineering Panda, Dillip; Clemson University, Department of Materials Science and Engineering

Silicon Oxycarbide Ceramics as Next Generation Anode Materials for Electrochemical Applications

Ravindran Sujith[a,b], Jella Gangadhar[a], Michelle Greenough[c], Rajendra K. Bordia[c]
Dillip K. Panda[c*]
[a]Mechanical Engineering Department, Birla Institute of Technology and Science Pilani, Hyderabad Campus-500078 (India).
[b]Materials Center for Sustainable Energy and Environment, Birla Institute of Technology and Science Pilani, Hyderabad Campus-500078 (India).
[c]Department of Materials Science and Engineering, Clemson University, Clemson, SC-29634, US.

*Corresponding Author **:** dpanda@g.clemson.edu

Abstract

Lithium-ion batteries (LIB) are the energy storage system of choice for the electrification of transportation and portable electronics. They are also being actively considered to meet the need to store electricity produced by renewable sources which tend to produce electricity intermittently. In commercial LIB, graphite is the most common anode material. However, its theoretical specific capacity (372 mAh/g) is limited. A search for alternatives led to the development of Si anodes due to their extremely high theoretical specific capacities (4200 mAh/g). However, its commercial viability is limited due to its high volumetric expansion (more than 300%), which results in capacity fading during cycling. Silicon oxycarbide (SiOC) materials, which are synthesized using a polymer-derived ceramic (PDC) route, are investigated as a substitute anode material for crystalline Si-based anodes. The specific capacity of these SiOC materials ranges from 200-1300 mAh/g. Further, these SiOCs are tailorable to meet the needs of electrochemical applications due to their versatile synthesis route. Moreover, the amorphous nature of these materials and their micro-mesoporous structure make them capable of accommodating large strains when charged or discharged. In this review, we discuss the various factors that influence SiOCs' electrochemical performance, storage mechanisms, and recent developments. SiOC anodes suffer from low electrical conductivity, low Coulombic efficiencies, large hysteresis, and high first-cycle losses. Several techniques, such as nanoparticles, prelithiation, and thin-film geometries, have been employed to overcome these limitations. Literature on these approaches is also reviewed. A number of recent studies have also examined the use of SiOC in lithium-tin anodes, sodium-ion batteries, and supercapacitors. The status of these developments and the challenges associated with the wide-scale use of SiOC is presented.

Keywords: Lithium-ion batteries; Polymer-derived ceramics; Amorphous materials; Energy storage; Electrochemistry; Supercapacitors; Graphene

Introduction

We are on the path to transitioning from internal combustion engine-based mobility to electric vehicles, and lithium-ion batteries (LIB) play an important role in achieving this target [1]. Compared to conventional lead-acid and nickel-cation batteries, LIB has gained considerable interest owing to their high energy and power densities, better safety, and long cyclic stability [2]. As an anode material, graphite is most commonly used in LIB. It has a theoretical capacity of 372 mAh/g in a lithiated state (LiC_6) [3]. The capacity mentioned above, however, is not sufficient to meet the ever-increasing global demand for higher energy densities, requiring the development of alternative materials capable of providing higher energy densities. Due to its high theoretical capacity of 4200 mAh/g and low working voltage of 0.4 V [4], Si has garnered much attention among possible alternatives. Although Si-based anodes are attractive, their applications are limited due to their high volumetric expansion (300%) and poor electrical conductivity. High volumetric strain leads to pulverization of Si-anodes leading to capacity fading in these cells [5]. Many efforts have been made, and are continuing to be made, to overcome this constraint, including nanostructuring and embedding Si particles in another matrix [6–12]. Although these efforts have been made, commercialising the Si anodes remains a substantial challenge, in part, because of their high fabrication costs, complexities in processing, and low volume production [13]. The properties of various materials employed as anodes in LIB are presented in Table 1.

Table 1: The properties of various materials employed as anodes in LIB.

S.No	Anode Materials	Theoretical Capacity (mAh/g)	Electrochemical Potential (V)	Volume Expansion (%)	Electrical Conductivity (S/m)	Density (g/cc)
1	Graphite [14,15]	372	0.1	13.2	1.2×10^5	2.25
2	Silicon [14,15]	4200	0.4	323	6.7×10^{-2}	2.30

3	Lithium [14,15]	3860	3.04	-	1.1×10^{7}	0.53
4	Lithium Titanium Oxide [14,15]	330	1.5	1	7.5×10^{-5}	3.43
5	Tin [14,15]	994	0.6	260	9.1×10^{6}	7.31
6	Antimony [14, 15]	660	0.9	200	2.5×10^{6}	6.68
7	Silicon oxycarbide	1300 (Maximum) [16]	< 0.5 [17]	22 [18]	3×10^{-8} - 2.2 [19]	1.80 -2.30 [20]

Compared to crystalline Si, silicon oxycarbides (SiOC) offer high structural stability, low volumetric expansion (22%), ease of fabrication, and large-scale production capability [21,22]. One of the most efficient methods for the synthesis of SiOC ceramics is the polymer-derived ceramic (PDC) route, wherein a sutable polymeric precursor is pyrolyzed in a controlled atmosphere to produce the required ceramic. It is possible to achieve a better control over the composition of the ceramic via PDC route compared to other processing routes such as sol-gel processing. The pyrolysed ceramics are typically amorphous in nature consisting of $SiO_{4-x}C_x$ tetrahedral units. The amorphous nature of the ceramics is crucial for battery applications as it can accomodate the volumetric strains during Li-ion insertion. In addition, depending on the polymeric precursor chemistry, a little or considerable amount of disordered carbon (free carbon) is produced during the pyrolysis process, which could act as efficient charge carriers and active sites for Li-ion insertion. Moreover, the presence of micro-mesoporosities provides an additional buffer for these PDCs to accommodate volumetric strains [23-25].

In the literature, SiOC anodes' capacities has been reported between 200 to 1300 mAh/g, likely due to structural differences in the SiOC ceramic used to fabricate these anodes. During the production of PDCs, precursor chemistry and processing parameters have a strong influence on the final phase composition and microstructure of the ceramic. A number of other factors have also been reported to influence the energy storage mechanisms of SiOCs, including the amount of free carbon, the fraction of tetrahedral units, and the porosity [26-29].

Although the specific capacity that can be achieved is double to that of the commercially existing graphite and there is the advantage of ease of processing, SiOC also faces other challenges as an anode material, including high first cycle irreversibility, voltage hysteresis, low electrical conductivity and lower capacity than pristine silicon. The main challenge is its low Coulombic efficiency (40-70%), especially during the first cycle, due to the irreversible nature of alloying reactions between Li and Si [4]. There is also a limitation of its low electrical conductivity, with values ranging from 10^{-5} S/m to 2 S/m depending on the amount of free carbon in the material and its structure [30]. Although free carbon can lead to better conductivity than pure Si, SiOCs have reported lower conductivities for LIB applications because of the open structure of free carbon and the lack of sufficient volume fraction of carbon necessary to form the desired perculating network [31]. Nevertheless, these limitations can be overcome by controlling the initial precursor chemistry and developing composite anodes [29,30,32,33]. Additionally, strategies such as pre-lithiation, synthesis of spherical and thin-film anodes etc, can enhance the reversible storage capacity and Coulombic efficiency of these systems [34,35].

In the literature, readers can find several detailed review papers on polymer-derived ceramics including their synthesis and characterisation [20,36–48]. To our knowledge, there have been no reviews that focus exclusively on SiOC's suitability as anodes in LIB and other electrochemical applications. The purpose of this review is therefore to discuss factors influencing the electrochemical properties of SiOCs, existing challenges, and strategies for overcoming them.

1. Synthesis of Polymer-derived Silicon Oxycarbide Ceramics

PDCs are synthesized by pyrolyzing polymeric precursors in a controlled atmosphere. Verbeek et al. were the first to demonstrate polymer to ceramic transformation by the pyrolysis route. They synthesied SiC by pyrolysis of polysilanes in a controlled atmosphere [49]. In later studies, Fritz and Raabe, Yajima and co-workers made significant breakthroughs in PDC synthesis [50]. A variety of silicon-based polymer precursors have been researched over the past 50 years, and figure 1 shows the families of the important polymeric precursors that have been used in the field of PDCs. Since SiOC ceramics are easy to synthesize and readily available, they have been gaining much attention [39]. Aside from that, these PDCs have shown excellent chemical and thermal stability, making them suitable for a variety of functional applications, including energy storage, high-temperature sensors, microelectromechanical systems, drug delivery, filters and catalysis [21,38,46,47].

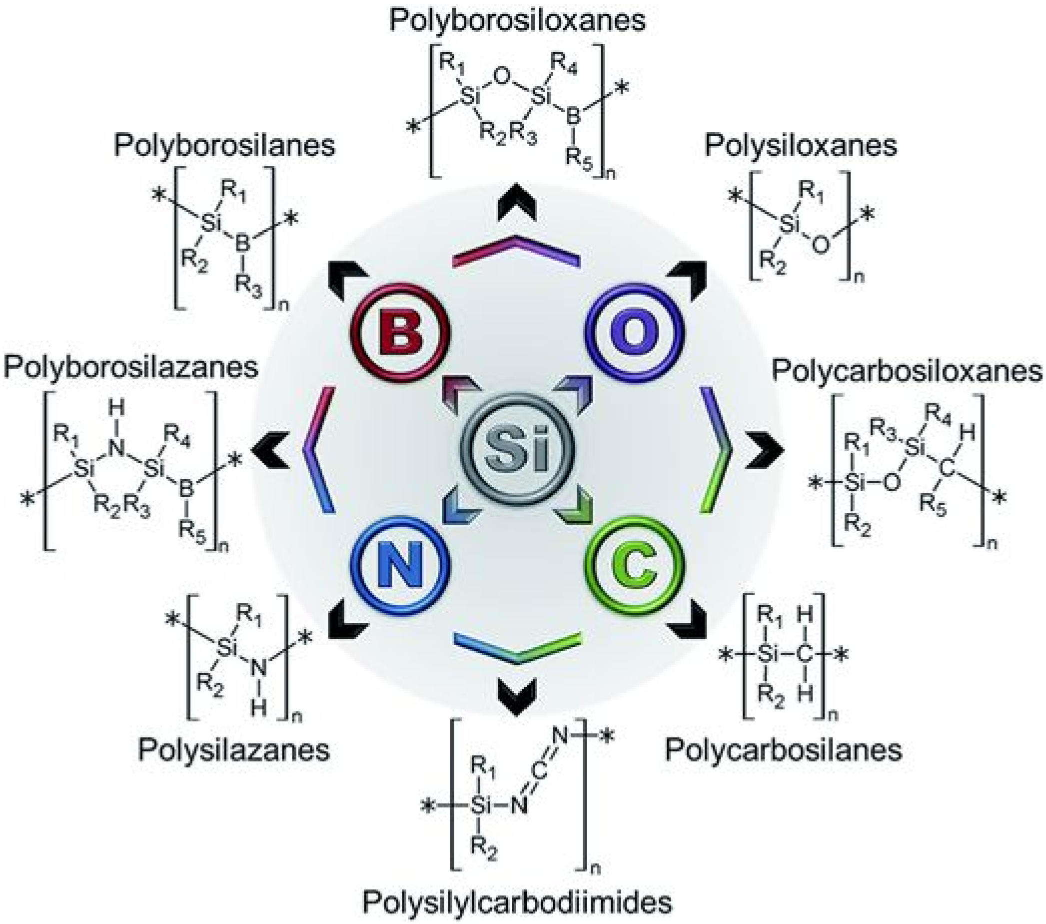

Fig. 1 Overview of the various polymeric precursors used in the synthesis of PDCs [39]. Reproduced with permission from ref. 39. Copyright 2019, Royal Society of Chemistry.

The ceramic obtained by the pyrolysis of a polysiloxane could result in an open network-like structure consisting of amorphous phases of SiOC with $SiO_{4-x}C_{x\ (x\,=\,1-4)}$ structural units and disordered carbon (free carbon) [20]. The final structure of the ceramic is controlled by the choice of the polymeric precursors and the processing parameters (e.g. method of crosslinking, pyrolysis temperature and atmosphere). The schematic representation of the synthesis procedure of polymer-derived SiOC ceramic is shown in figure 2. It is possible to customize the final ceramic material using the parameters provided in the schematic (Figure 2). In addition, with increasing pyrolysis temperatures (>1200°C), carbothermic reduction could take place resulting in phase separation and crystallization of SiOC [51–53], which may be unsuitable for battery applications.

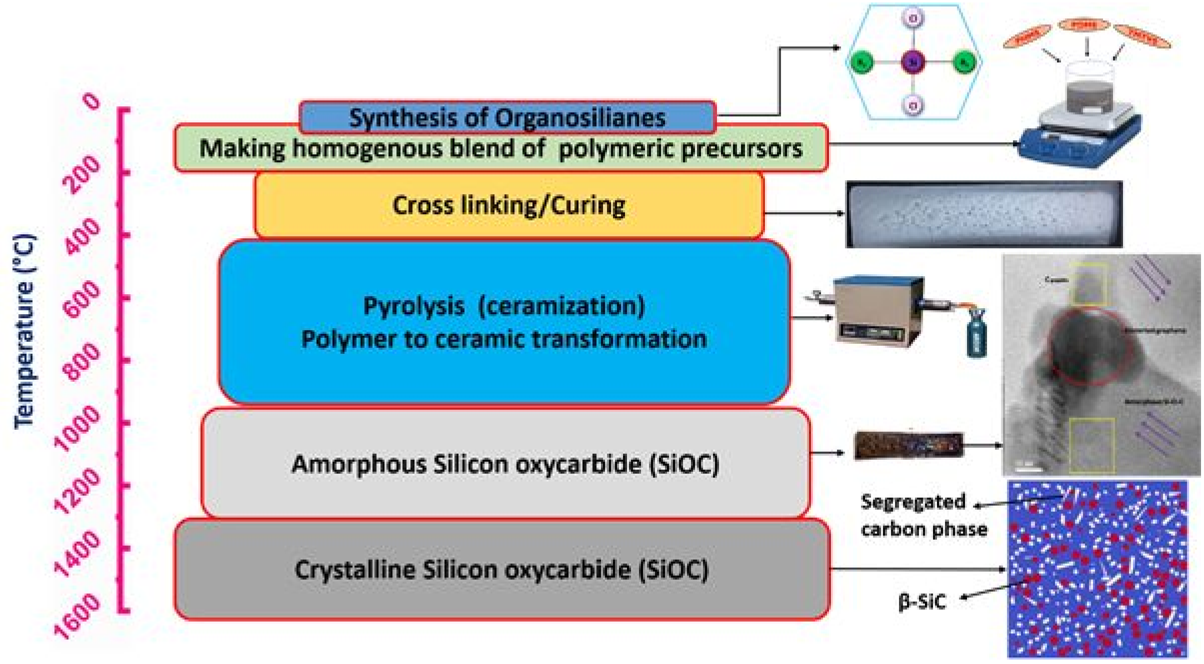

Fig. 2 Schematic illustration of synthesis procedure of polymer-derived silicon oxycarbide ceramic [38,39,54]. In designing the schematic, the idea was taken from references 38, 39. TEM image is reproduced with permission from ref. 54 Copyright 2018, Springer Nature. SiC segrated carbon phase image reproduced with permission from ref. 52, Copyright2018, MDPI.

In general, the precursors used to synthesize SiOC PDCs can be classified into Si-rich and C-rich precursors to better comprehend the mechanisms of their energy storage. For achieving C-rich SiOC, various strategies have been employed, including the use of precursors that have phenyl groups [28,55,56], and the addition of divinylbenzene (DVB) [57,58]. In spite of this, there may be a threshold limit beyond which free carbon becomes destabilised [58]. Therefore, it is imperative to control the size of free carbon domains. A study found that DVB facilitates the formation of free carbon and silicon oxycarbide bonds [57]. Further, the presence of free carbon could be beneficial to the fabrication of LIB as it improves their electrical conductivity [30]. A silicon-rich SiOC can be synthesized through the pyrolysis of polymeric precursors such as tetraethoxysilane, polyhydroxymethylsiloxane, cyclic 2,4,6,8-tetramethyl-2,4,6,8 tetravinlycyclotetrasiloxane,1,3,5,7-tetramethyl-1,3,5,7-tetravinylcyclotetrasiloxane (TTCS) and silicone oil. SiOC systems would be predominantly silicon-rich if silicon-based polymeric precursors did not contain phenyl or alkyl groups in the precuror. However, it should be noted that the Si-rich SiOCs contain free carbon, albeit in low concentrations [57].

The porosity of PDCs also plays a key role in determining their usefulness as anodes for LIB. As a result of the escapement of various volatile materials during pyrolysis, PDCs are inherently porous. By tuning the process parameters and modifying precursor chemistry, it is possible to achieve the desired porosity levels [43]. Porosity can be further tuned to the desired level by employing various strategies such as hydrofluoric acid etching, infiltration, and use of sacrificial template techniques [17,24,59–63]. It has been observed that the porosity improves the cyclic stability of LIB by accommodating the volume expansion. However, high level of porosity compromises transport of Li-ions and mechanical properties. Thus, there is a requirement for synthesising SiOCs with optimum level of porosity [23,29].

3. Mechanisms of electrochemical storage

The Li-ion storage in SiOC typically exhibits a dual mechanism involving intercalation and alloying processes (Figure 3a,b). The presence of silica tetrahedral units facilitates alloying whereas the free carbon facilitates intercalation. Depending on whether the material is silicon rich or carbon rich, the dominant mechanism can be illustrated. Liu et al studied the mechanism of SiOC by performing various characterization techniques such as ^{29}Si magic angle spinning nuclear magnetic resonance (NMR), Si X-ray photoelectron spectroscopy and cyclic voltammetry [64]. In their study they have postulated that there exist four species/resonances in the SiOC sample such as SiO_4, SiO_3C, SiO_2C_2 and $SiOC_3$, out of which SiO_3C, SiO_2C_2 are electrochemically active to Li-ions and contribute towards reversible capacity whereas $SiOC_3$ is irreversibly converted into SiC_4 after the first cycle. The active SiO_4 phase resulted in Li_2SiO_3 on intercalation, whereas the inactive part resulted in Li_4SiO_4. Studies by Xue et al. showed that irreversible capacity, associated with the initial cycle charge/discharge of a SiOC increases with the increase of silicon and oxygen contents [65]. Contrary to Liu et al, other studies have showed that the carbon phase is the major Li-ion storage host site. It has been shown that lithium is accommodated in interstitial and defect sites, edges of graphene sheets, and adsorbed on the interface of graphite nano-crystallites in carbon-rich SiOC [24,27,66-68]. Further, 7 Li-MAS NMR measurements performed by Fukui et al confirm the presence of at least two electrochemically active sites for lithium storage in the SiOC composite materials, out of which the carbon phase is the major host site for lithium storage [69]. Additionally, extensive structural and electrochemical studies reveal that the micropores present in SiOC can act as active sites for lithium storage resulting in better reversibility in the range 0.005−0.4 V.

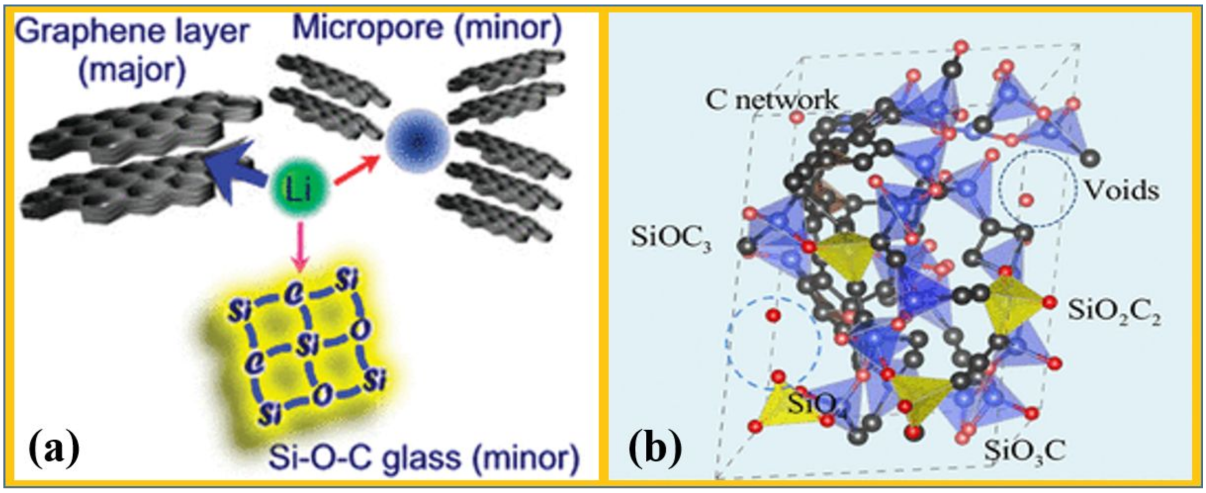

Fig. 3 Mechanism of Li-ion storage in SiOC for (a) carbon rich [66] and (b) silicon rich material system[18]. Reproduced with permission from ref. [66]. Copyright 2010, Reproduced with permission from ref. [18]. Copyright 2017. American Chemical Society.

4. First principle studies

Studies based on the first principle revealed that atomic structure and bonding mechanism play an important role in the lithiation process [18,70-74]. The insertion of Li-ion in SiOC ceramics with different carbon contents was investigated by Liao and co-workers using density functional theory (DFT) calculations [70]. Figure 4 illustrates the lithiated state of the various structures. It is concluded from their study that the Li atom prefers to bond with oxygen atoms and stays near carbon atoms in the empty spaces. Therefore, based on their research, it can be concluded that high carbon content results in better reversible storage capacities, which is supported by experimental observations [70]. In addition, DFT studies have shown that carbon in the segregated form stabilises the whole system by forming 3D networks. They have also calculated the formation energy of the lithiated systems and reported the most stable composition for $Li_xSiC_{2/5}O_{6/5}$, $Li_xSiCO_{6/5}$, and $Li_xSiC_{8/5}O_{6/5}$ are x = 2.75, 3.25 and 4. These correspond to theoretical specific capacities of 1415, 1470 and 1613 mAh/g, respectively [74]. SiOC has also been found to have a favorable lithium insertion process than SiO_2, possibly because it has a larger free volume than SiO_2 [72]. A similar study by Sun and Zhao et al on the the atomistic origin of the performance of carbon-rich SiOC, which demonstrates a two-step process of lithium insertion: (i) Li ions adsorb into nano-voids followed by (ii) accommodation of the Li ions in the SiOC, segregated carbon network and the defect sites. They have also observed that a maximum volumetric expansion of 22% can occur in these systems at the fully lithiated capacity of 1230 mAh/g [18]. Kroll et al. also found that the storage of lithium ions in amorphous silica and SiOC without segregated carbon is energetically unfavourable because of a large bandgap, whereas the bandgap of SiOC ceramics can be reduced considerably by the presence of the low-laying unoccupied states arising from the free carbon phase [75]. Further, it is also ascertained that the free carbon facilitates lithium ions bonded to oxygen sites via improving the electronic conduction, leading to irreversible lithium uptake. On the other hand, the free carbon also contributes to a major part of the reversible lithium storage capacity.

Further, first principle studies on five different SiOC structures have shown that Li_2O tends to form initially due to the cleavage of Si-O, and later Li_xO and Li_ySi form with increasing lithium-ion concentration [70]. Interestingly, carbon does not attract lithium-ions in such systems but stabilizes them by forming stable C-C bonds. They have also reported that the free volume decreases with the carbon content; hence, the voids have an insignificant role in its better electrochemical performance. Further, as observed experimentally, the reversible capacity increases with increasing carbon weight fraction, but beyond a threshold value, it tends to decrease with an increase in carbon content [70]. However, another study revealed that, at least initially, the Li-ions occupy the microvoids present in SiOC. Subsequent insertion could lead to the cleavage of Si-O and Si-C, leading to larger free volumes [71]. They have also estimated the theoretical storage capacities in O-rich $SiO_{1.5}C_{0.5}$ and C-rich $SiO_{0.5}C_{1.5}$, and the corresponding values were, Li^+ is 519 and 681 mAh/g; Na^+ is 335 and 186 mAh/g; K^+ is 335 and 681 mAh/g, respectively. The repulsion-created structural instability is the reason for K^+ions' relatively low storage capacities, whereas favourable Li-Si formation is responsible for the higher storage capacity of Li^+ ions [71]. However, it has been reported that local compressive stresses are generated in the lithiated systems resulting in the shortening of bond lengths and higher bulk modulus [76]. This also means that the local stress generated can be used to measure the system's specific capacity. Moreover, it is observed that replacing oxygen with nitrogen in these systems makes it unattractive for lithium intercalation due to the high covalent nature of Si-N bonds and the lower electron density of nitrogen atoms [77]. Hence, silicon carbonitrides are expected to exhibit lower storage capacities in comparison to silicon nitrides and experimental evidence also supports this [78-80].

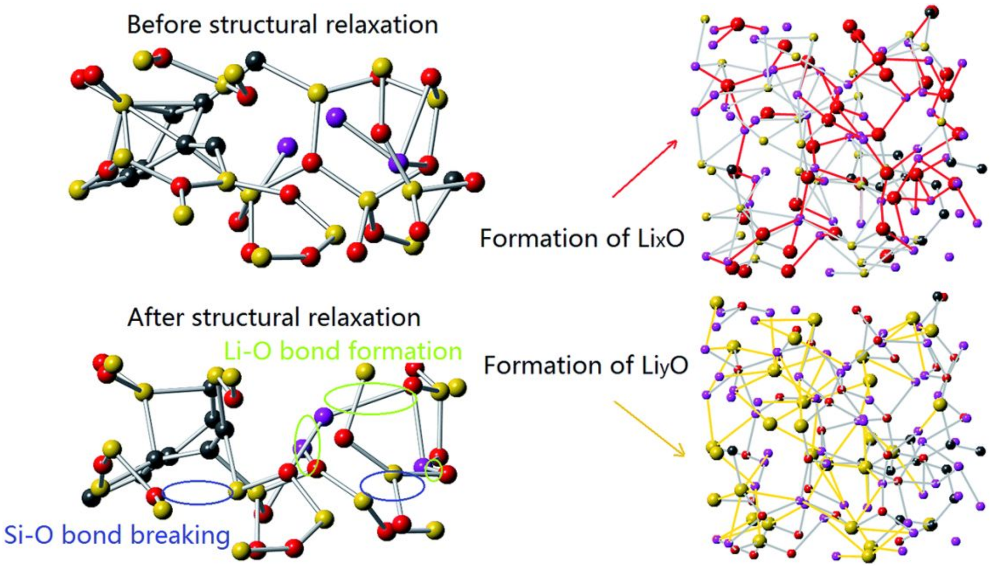

Fig. 4 The zoom-in structures of lithiated $SiC_{2/5}O_{6/5}$. The left picture is about Li incorporation through the breaking of Si–O bonds and the formation of Li–O bonds, and the right image describes the formation of Li_xO and Li_ySi complexes [70]. Reproduced with permission from Ref. 70. Copyright 2016, Royal Society of Chemistry.

5. Factors affecting the electrochemical properties of SiOC anodes

5.1 Presence of free carbon

Anodes fabricated out of amorphous SiOC ceramics prepared by the thermolysis of phenyl-substituted branched polysilane ($(Ph_2Si)0.85(PhSi)0.15$) and polystyrene (1:1 by weight) have shown a capacity of more than 600 mAh/g. In these systems, the Li-ion is electrochemically stored in the interstitial spaces of the free carbon in the SiOC phase and the micropores. The system chosen was C-rich, thus the interlayer spacing within the free carbon contributed more to electrochemical storage, suggesting an increase in free carbon content might be able to increase the storage capacity of the battery [17]. Furthermore, other studies have also shown that free carbon in the disordered form offers higher Li-ion storage sites in comparison to ordered free carbon [55,57]. Wilamowska and co-workers synthesised SiOC ceramics with varying carbon content (from 25 to 40 wt.%) and demonstrated that the reversible capacity improves with the carbon content. However, there seems to be no linear relation between the free carbon content and its electrochemical performance [55]. Contrary to the previous observation Monika and co-workers demonstrated a linear dependence between the carbon content and its electrochemical performance. Carbon-rich samples exhibited much higher capacities (550 mAh/g at low C rates after 140 cycles) and lower irreversible capacities (360 mAh/g) than carbon-lean samples [26]. Thus, free carbon in the disordered form is crucial to improving the electrochemical performance of SiOC.

Free carbon has an additional important effect of increasing the electrical conductivity. It was observed that at a carbon content less than 20 wt.%, electrical conductivities were less than 3 x 10^{-5} S/m. However, the electrical conductivity of the material was improved to 2.2 S/m by increasing the free carbon content to 54 wt% [30]. In this regard, Kaspar and coworkers noted that a lower carbon content might lead to a lower electrical conductivity and therefore higher irreversibility. This conclusion was reached after observing that the low electrical conductivity system initially showed an initial storage capacity of 1000 mAh/g, but then it rapidly diminished with subsequent cycles. In the high electrical conductivity systems, the initial storage capacity was lower, but the observed capacities (500 mAh/g) remained stable after 60 cycles [30]. So, it can be concluded that the presence of free carbon improves the electrical conductivity and cyclic stability of SiOC anodes.

The role of free carbon in the electrochemical properties of SiOCs was later systematically determined by Pradeep and coworkers [16]. In their study, they synthesized amorphous SiOC ceramics with free carbon contents ranging from 8 to 50 wt.%, maintaining the same O-to-Si atomic ratio. Unlike studies mentioned earlier, their study revealed that SiOC tetrahedral units have a greater impact on reversible capacity than free carbon. Additionally, they observed a linear relationship between SiOC units and Li insertion capacity, which is consistent with the model proposed by Raj and co-workers [81]. Nevertheless, their studies also indicate that 0.5 wt.% of free carbon should be present in the system to achieve the desired levels of electrochemical performance. Therefore, it is important to consider both SiOC units and free carbon content when determining a system's storage capacity.

5.2 Microstructure of PDC

There have been several studies carried out using different types of precursors to understand the effect of compositional differences on the reversible storage capacities of SiOCs [28]. According to Halim and co-workers, SiOC was synthesized from phenyl-rich silicone oils and showed a discharge capacity of 800 mAh/g at a current density of 200 mA/g. Its better performance is due to its low dimensional expansion (about 7%) during lithium cycling as well as its enhanced mobility of Li^+ within the matrix (Diffusivity of Li^+: 5.1 x 10^{-6} cm^2/s) [28]. Further, it was shown that O-rich SiOC maximises reversible storage capacity more than C-rich counterparts [82]. It could be possible because the SiOC tetrahedral unit dominates the free carbon network.

Another significant aspect that influences the electrochemical performance of SiOC systems is the type of Si-C bonds.Graczyk- Zajac and co-workers synthesised SiOC by pyrolysing polysiloxanes in two different atmospheres - CO_2 (oxidising) and Ar (inert) [83]. NMR studies on the PDC synthesised in the oxidising atmosphere revealed the absence of Si-C bonds, whereas the PDC synthesised in inert conditions contained C_2SiO_2, $CSiO_3$ and SiO_4. Moreover, the respective free carbon contents in both the ceramics were 37 wt% and 47 wt%. Interestingly, both these systems showed the same initial storage capacity of 1500 mAh/g during the charging. However, the reversible capacity of the Ar-treated sample (~ 800 mAh/g) was found to be much higher compared to the sample treated under oxidising conditions (~600 mAh/g) [83]. A high concentration of reversible oxygen-containing species such as SiO_4 and SiO_3C may also contribute to the high reversible storage capacity. This characteristic behavior is probably explained by the high ionic character of the Si-O bonds [64].

5.3 Pyrolysis temperature

In a similar vein, the significance of pyrolysis temperature on battery performance is unclear. Ahn and Raj have demonstrated the necessity of mixed bonds for achieving high levels of Li-ion insertion in PDCs [84]. Their study showed that pyrolysis at 1000°C achieved the maximum reversible storage capacity of 958 mAh/g. In contrast, the samples processed at 1400°C showed only 88 mAh/g of reversible storage capacity [64]. Other studies have also observed a rapid decline in storage capacity as the pyrolysis temperature increased [68]. For instance, Kaspar and co-workers demonstrated that SiOC pyrolysed at 1100°C exhibited a stable 521 mAh/g reversible capacity. On the other hand, the one pyrolyzed at 1300°C exhibited a storage capacity of only 367 mAh/g. There have been reports of the formation of several crystalline phases by pyrolysis at temperatures greater than 1200°C, including SiC, SiO_2 and ordered carbon [85–88]. Since SiO_2 and SiC are inactive species and do not contribute to Li storage, such formation of crystalline phases would reduce storage capacity [89]. A similar study by Riedel's group supports the finding that lithium's storage capacity decreases with increasing pyrolysis temperatures.These deteriorating properties can be attributed to three main reasons: (i) ordering of free carbon, (ii) lower structural stability of free carbon because of phase separation in SiOC and (iii) crystallisation of electrochemically inactive phases like SiC [89]. Furthermore, NMR studies confirmed that ceramics pyrolyzed at high temperatures (1400°C) contained electrochemically inactive species like SiC_4 [55]. One study, however, reported that the SiOC pyrolysed at 1300°C exhibited a better reversible storage capacity of 780 mAh/g as compared to the low-temperature pyrolysed system [16]. In their study, they attribute the superior performance of high-temperature pyrolysed SiOC to its exceptional thermodynamic stability, which makes it less prone to reactive reactions with Li [16]. It is interesting to note that from the cyclic stability standpoint, the samples pyrolysed at 800 °C showed a better Coulombic efficiency of 100% and could last 60 cycles compared to samples pyrolyzed at 1000 °C [84]. It is well known that the residual hydrogen content decreases as the pyrolysis temperature increases. Thus, samples pyrolyzed at 800 °C should contain more residual hydrogen than those at 1000 °C. The hypothesis is that this excess residual hydrogen stabilizes the material [84]. It has also been observed that thermal crosslinking before pyrolysis improves the reversible storage capability. Using thermal crosslinking at 400°C to synthesize C-rich SiOC, Kaspar and co-workers studied its electrochemical performance. They observed crosslinked systems performing better than directly pyrolysed samples [87]. A summary of the effect of precursors and pyrolysis temperature on the electrochemical performance of SiOC ceramics is shown in Table 2.

Table 2 Electrochemical performance details of SiOC ceramics as anode materials synthesised from various polymeric precursors and the temperature of pyrolysis.

S.NO	Specimen (current density mA/g)	Synthesis temperature (°C)	Polymeric precursor	First reversible capacity (mAh/g)	First cycle loss (%)	Reversible capacity (mAh/g) (after N cycles) (Current density (mA/g))	Reference
1	SiO_2rich dense SiOC. (18) Porous SiOC HF etched (18)	1400	poly(methylhydrosiloxane)PHMS, 200% divinylbenzene (DVB)	241 268	60 58	0 (10 cycles) Stable (30 cycles)	Dibandjo et al 2012[24]
2	Carbon rich SiOC- Ar (18) Carbon rich SiOC- Ar /H_2 (18)	1000	PHMS, 200%DVB	568 704	37 33	372 @ 2-C (50) < 200 @ 2-C (50)	Pradeep et al 2013[90]
3	SiOC -PD2 (18.6)	1100	Polyramic RD-684a, DVB	603	39	200@ 1-C (100)	Liu et al 2013[58]
4	PD2 (18) PT2 (18)	1000 1300	Low C= PHMS+TMTVS High C= PHMS+DVB	656 728	41 32	600 (130) ~400 (130)	Pradeep et al 2014[16]
5	SiOC (70)	1000	PHMS, DVB	862	26	-	Fukui et al 2014[17]
6	Carbon rich SiOC (360)	1000	PHMS, 200%DVB	650	47	600 (100)	Pradeep et al 2015[25]
7	PR/DVB 50/50 (37) PR (37) RR (37) SR/RR 50/50 (37) SR/RR 25/75 (37) Carbon rich SiOC	1000	Polyorganosiloxnes (RD-684a (PR), RD-688 (RR), RD-212 (SR), polysilsesquioxane PMS MK, DVB	504 535 434 501 682	36 38 39 38 42	338 (60) 304 (60) 255 (60) 237 (60) 91 (60)	Kaspar et al 2016[30]
8	SiOC- Ac/Ar (360) SiOC Ac/ H_2(360) SiOC Cy/Ar(360) SiOC Cy/ H_2 (360)	900	PHMS, 200%DVB	763 919 332 495	49 50 65 48	570 (250) 604 (250) 307 (250) 477 (250)	Pradeep et al 2016[91]
9	SiOC- Ar (36) SiOC- CO_2 (36)	900	PHMS, 200%DVB	~760 ~580	50 63	> 400 (100) > 200 (100)	Graczyk-zajac et al 2018[83]
10	SiOC-P0 (72) SiOC-P1 (72) SiOC-P2 (72) SiOC-P2 (72)	900	PSS-Octakis(dimethylsilyloxy) substituted (POSS), PHMS, DVB				Lee et al 2020[82]

11	SiOC-DVB-1 (100) SiOC-DVB-2(100) SiOC-DVB-3(100) SiOC-DVB-4(100)	1200	polymethylsilsesquioxane (PMSQ), DVB	819 929 892 780	35 36 32 34	476 (500) 463 (500) 435 (500) 273 (500)	Wu et al 2022[92]
12	SiOC- KF-54 (50) SiOC-105 (50) SiOC-103 (50) SiOC-101 (50)	900	KF-96 silicon oil, DVB	461 412 532 829	47 47 47 38	90 % capacity retemtion in all sample (500)	Lim et al 2021[57]
13	SiOC- PhTES (18.6) SiOCPhTES:MTES 2:1 (18.6) PhTES:MTES 1:1 (18.6) PhTES:MTES 1:2 (18.6) MTES (18.6)	1000	Phenyltriethoxysilane (PhTES) methyltriethoxysilane (MTES)	652 842 939 685 303	39 37 39 35 75	80% capacity retention (140)	Wilamowska et al 2014[55]
14	SiCO_Ph (50) SiCO_Ph_M (50) SiCO_Ph_T (50)	1000	PhTES, MTES & TEOS	538 745 858	49 33 27	- - 400 @0.5 A/g (100)	Weinberger et al 2015[93]
15	Me-SiOC (35) Vi- SiOC (35) Vi-Ph-SiOC (35)	1100	Methyltrimethoxysilane (MTMS; 97%), vinyltrimethoxysilane (VTMS; 99%), and phenyltrimethoxysilane (PTMS; 97%	761 789 922	47 38 23	241 (100) 299 (100) 747 (100)	Krüner et al 2018[4]
16	PVA-SiOC (100) P-SiOC (100)	900	PhTES, PVA	595 533	39 54	505 (150) 235 (100)	Shi et al 2019[94]
17	H-SiOC-900 (50)	900	PhTES, TEOS	1115	25	961 (50), 480 @ 500 mA/g (200)	Xia et al 2021[95]
18	DDTS-SiOC (50) DTDS-SiOC (50 TPTS-SiOC (50)	800	1,5-divinyl-3,3- diphenyl-1,1,5,5-tetramethyltrisiloxane (DDTS), 1,3- divinyltetramethyldisiloxane (DTDS), 1,3,5- trivinyl-1,1,3,5,5-pentamethyltrisiloxane (TPTS)	866 800 636	28 48 48	580 (50) 800 (50) 100 (50)	Mujib et al 2021[96]
19	SiOC-1000 (100) SiOC-800 (100)	800	1,3,5,7-tetramethyl-1,3,5,7-tetravinylcyclotertrasiloxane (TTCS)	958 906	23 33	95% (60) 100 % (60)	Raj et al 2011[84]
20	SOC-HF (200) SOC (200)	950	1,3,5,7-tetramethyl-1,3,5,7-tetravinylcyclotertrasiloxane (TTCS)	568 300	42 47	573@200 mA/ g 544@500 mA/ g 233@200 mA/ g 193@200 mA/ g (100)	Ma et al 2016[62]

21	SiOC P_{1AC1} (37) SiOC P_{2AC1} (37)	1000	acenaphthylene $(Ph_2Si)_{0.85}(PhSi)_{0.15}$ and $(MePhSi)_{0.70}(Ph_2Si)_{0.15}(MeSi)_{0.15}$,	498 580	33 32	(40 (40)	Fukui et al 2011[67]
22	SiOC PP-700 (74) SiOC PP-900 (74) SiOC PP-1100 (74)	700-1200	Polystyrene Phenyl substituted polysilane $(Ph_2Si)_{0.85}(PhSi)_{0.15}$	795 576 517	37 39 36	Improved @37mA/g (30) For all samples	Fukui et al 2013[68]
23	SiOC -1100 (37) SiOC -1300 (37)	1100 1300	Polyramics RD-684 (SiOCRD684)	572 374	39 43	521@37mA/g (75) 367@37mA/g (75)	Kaspar et al 2012[87]
24	SiOC -1100 UV curing (37) SiOC -1300 UV curing (37)	1100 1300	Polyramics RD-684 (SiOCRD684)	658 532	39 43	630 (18.5) (350) -	Kaspar et al 2012[27]
25	SiOC (100) Si/ C composite (100)	900	Dimethylpolysiloxane, poly(dimethylsiloxane-co-methylphenylsiloxane)	676	-	800 @200 mA/g (250) 222 @200 mA/g (250)	Halim et al 2016[28]
26	SiCO_1.3 (50) SiCO_0 (50)	1000	Silicon tetraacetate, Citric acid	563 217	56 78	422 @ 200 mA/g (200)	Tahir et al[97]
27	SiOC BPO-C (50)	1000	4,40 -bis(triethoxysilyl)-1,10 –biphenyl, triblock copolymer Pluronic P123	674	50	600 @ 50 Ma /g (200)	Weinberger et al[29]
28	SiOC H44 (50) SiOC MK (50) SiOC RSN (50)	1000	methyl -phenyl-siloxane H44 MK methyl-siloxane MK, phenyl-siloxane RSN	578 243 60	46 10 90	~360 @100 mA/g < 100 for MK AND RSN @100 mA/g (50)	Mujib et al[98]
29	SiOC-500 (100) SiOC 600 (100) SiOC 700 (100)	500 600 700	rose pollen grains, tetraethyl orthosilicate (TEOS)	578 657 284	43 36 55	351 (200) 275 (200) 220 (200)@100 mA/g	Xia et al[99]

6. Strategies to improve the battery performance

6.1 Enhancing the electrical conductivity

Among the major challenges limiting the use of SiOC anodes in LIB is their low electrical conductivity. Even though disordered carbon is commonly found in these systems, their discrete distribution in the SiOC matrix and disordered structure result in poor conductivity [82,100,101]. The solution to this problem is to produce composite anodes with SiOC mixed with various carbonaceous nanomaterials such as graphite [102–105], carbon nanotubes [32,106,107], carbon nanofibers [13,108–110], graphene [33,111–119] and reduced graphene oxide [120,121]. Graphene, however, is widely explored among these carbonaceous materials due to its high electrical conductivity [31,54,101]. Table 3 shows the electrochemical performance of various carbon-based SiOC composites.

Table 3 Electrochemical performance of the carbon based SiOC composites.

Specimen (current density mA/g)	Synthesis temperature (°C)	First reversible capacity (mAh/g)	First cycle loss (%)	Reversible capacity (mAh /g) (after N cycles) (Current density (mA /g)	Reference
Carbon based SiOC					
SiOC:C nanofiber (50)	700	839	27	669(80)	Li et al (2014)[109]
SiOC:Cnano hybrids (50)	800	436	46	470 (50)	wanget al 2016[122]
SiOC/C NF-0.5(100)	1000	1011	32	707(200)	Huang et al (2021) [13]
SiOC/PAN nanofiber (372)	1000	778	29	715(200)	Li et al (2021)[108]
SiOC:CNT (100)	1000	948	35	846(40)	Shen et al (2011)[106]
SiOC−CNT paper (8.5)		539.6	54		Bhandavat et al 2011[32]
SiOC−CNT-5 (0.1 C)	1000	841	32	686 (40)	Bhandavat et al 2013[107]
onion-like SiOC/C (100)	900	658	22	540 (50) 365 (500) 2 A/g	Lin et al 2021[35]
Graphite based SiOC Composite					
GF-SiCO (93)	800	220	20	180 (350)	Saleh etal 2016[105]
SiOC/Graphite (SG) (50)	1000	580	29	480 (1000) (0.5 A/g 184 (1000) (2 A/g)	Wu etal 2019[106]
NCG@SiOC (372)	900 1100 1300	380 520 300	- 28 -	170 (100) @ 10-C (100) 300 @5-C, 200@10-C (1000) 173 (100(10-C (100)	Hong et al 2020[122]
SiOC$_{PhTES}$/C2$_{g}$ (186) SiOC$_{PhTES}$/C5$_{g}$ (186)	1000 1000	472 460	40 42	214@5-C, 4230.5-C (20)	Knozowski et al 2020[103]

SiOC$_{\text{PhTES}}$/C10$_g$ (186)	1000	452	46	242@5-C, 4080.5-C (20) 293@5-C, 3730.5-C (20)	
SiOC$_{\text{VTES}}$/ C2$_g$ (186) SiOC$_{\text{VTES}}$/ C4$_g$ (186) SiOC$_{\text{VTES}}$/ C10$_g$ (186)	1000 1000 1000	730 630 476	30 30 29	519 (270) 464 (270) 341 (270)	Knozowski et al 2021[104]
Graphene oxide/ reduced graphene oxide/ Graphene based SiOC Composite					
LBL-SiOC-rGO (50)	800	780	-	400 (30)	Kolathodi et al 2016[112]
SiOC/rGO (100)	-	635	45	507(50)	Islam et a 2016[120]
SiOC@C/graphene(200)	950	674	38	691 (100) 676 (200)	Ma et al 2022[113]
[109]SiOC:exfoliated graphite	1000	530	54	357 (20)	Ji et al (2009)[115]
10SiOC/graphene (50)	800	607	37	582 (90)	Ren et al (2015)[114]
60SiOC (100)	1000	702	32	588 (1020)	David et al 2016[115]
3D GNS SiOC (100)	`1000	844	34	701(100)	Sang et al 2018[117]
3D GNS SiOC$_f$(100)	1000	929	21	775 (100)	Sang etal 2020[116]
NGA SiOC 25 (37)	900	747	33	605 (90)	Shao et al 2020[118]

A composite anode comprising graphene nanosheets and SiOC was synthesized by Ji and co-workers and they were able to demonstrate a reversible discharge capacity better than graphite and monolithic SiOC [115]. These composite anodes exhibited an initial discharge capacity of 1141 mAh/g, but the discharge capacity decreased significantly after eight cycles to 364 mAh/g. Nevertheless, they have correlated the enhanced battery performance of these composite anodes to the formation of the new electrochemically active species, such as O_xSiC_y, at the interface between graphene and SiOC. Further, their X-ray photoelectron spectroscopy studies also indicated the formation of inactive species like SiC_4, but in smaller quantities. It is interesting to observe that the discharging capacity has shown an almost linear increase (173 mAh/g to 357 mAh/g) with the increase in the weight fraction of graphene nanosheets (4 wt.% to 25 wt.%), albeit an optimum weight fraction of graphene nanosheets was not discussed [115]. Similarly, David and co-workers fabricated self-standing anodes consisting of silicon oxycarbide in a matrix of reduced graphene oxide to get the components' synergistic effect [33]. Reduced graphene oxide serves as a percolation network, which increases electrical conductivity, whereas amorphous SiOC particles increase lithium storage. The paper electrodes they developed have shown a storage capacity of ~ 588 mAh/g at the 1020th cycle. Another advantage of such paper-based electrodes is that they provide enormous flexibility and have great potential for developing flexible devices [33,116]. In another study, it was demonstrated that embedding SiOC in graphite flakes' electrical conductivity and structural stability can be significantly improved [102]. They have achieved a reversible storage capacity of 500 mAh/g after 1000 cycles. Their study also showed that in such systems, a significant improvement in diffusion coefficient can be achieved by shortening the Li-ion diffusion paths. A diffusion coefficient of 2.0 x 10^{-10} cm^2/s was obtained, which is the highest value reported in the literature so far. Similar studies with carbon nanotubes have shown that a stable storage capacity of 686 mAh/g can be achieved at an average Coulombic efficiency of 99.6% [107]. It was also proposed that by nitrogen doping and by creating defects in carbonaceous fillers it is possible to enhance the electrical conductivity and electrochemical performance [13,110].

The previous discussion was on the external addition of carbonaceous materials. However, it is also possible to develop anode materials with better battery performance by in-situ synthesis of carbon-containing silicon oxycarbide nanocomposites [109]. 1D-SiOC/C composite nanofibers synthesised via electrospinning and pyrolysis route have a stable discharge capacity 70% higher than the Si/C nanofiber anodes. In this study, they achieved the necessary carbon content by adding polyacrylonitrile during the synthesis stage. It is to be noted that the requirement of adding carbon black or binders is unnecessary in such systems, thereby leading to better material usage [109]. In another study, the microstructure of the SiOC ceramics was modified withacenaphthylene to produce materials with high C content. However, increasing the concentration of acenaphthylene also deteriorated battery performance due to the higher content of free carbon. An interesting phenomenon observed during delithiation is a pseudo-voltage plateau that needs to be explored further [67].

In place of carbonaceous materials, other elements like tin [123–126], antimony [127,128] and in some cases transition metal dichalcogenides based on $MoSe_2$ [129] were explored as active fillers in improving the overall battery performance of SiOC anodes. The addition of Sn and Sb enhances the battery performance of SiOC anodes due to their high electrochemical activity. In the case of Sn, it was found that its presence limits the formation of electrochemically inactive SiC domains in the material system. In contrast, the addition of Sb seems to modify the structure of SiC, creating more favourable sites. However, the excessive addition of Sn or Sb particles may limit its performance due to the high volumetric expansion of Sn upon lithium insertion. Nevertheless, synthesising PDCs withexcessive free carbon could stabilise such systems [126]. Another primary concern with the addition of tin - especially in the case of in-situ inclusion of Sn by carbothermal reduction of SnO_2 - is its consumption of free carbon during the synthesis process. This reduces the structural stability of such systems. Hence, to circumvent this problem, graphite particles can be added externally [124]. An evaluation of crystalline and amorphous silicon nanofillers on battery performance was conducted, and crystalline nanosilicon embedded systems were found to have a better storage capacity (905 mAh/g) than amorphous silicon embedded systems (704 mAh/g). However, amorphous silicon embedded systems deliver better performance when it comes to cyclic stability. The nanosilicon particles under 10 nm are believed to have contributed to this better matrix integrity [130]. This paper also curiously mentions the possibility of improving the intrinsic electrical conductivity of nanosilicon-embedded systems due to the formation of SiC. However, such an improvement could potentially deteriorate battery performance because SiC is electrochemically inactive [89]. The electrochemical performance of various SiOC composites with non-carbonaceous fillers are presented in Table 4.

Table 4 Electrochemical performance of SiOC composites with non-carbonaceous fillers.

Specimen (current density mA/g)	Synthesis temperature (°C)	First reversible capacity (mAh/g)	First cycle loss (%)	Reversible capacity (mAh/g) (after N cycles) (Current density (mA /g)	Reference
Si/SiOC composites					
Si/Si–O–C (50)	1100	1372	22	990 (30)	Liu et al 2012[131]
SiOC. N –Si-a (74) SiOC. N –Si-c (74)	1100 1100	704 905	- -	620(100) 314(50)	Kaspar et al 2014[130]
Si@SiOC (100)	800	2093	29	2093 (200)	Choi et al 2014[132]
Si_{tc}: SiOC Si_{tc}:30C: SiOC Si_s: SiOC Si_s:30C: SiOC	1100	593 533 450 484	35 39 40 44	289 (50) 575 (50) 482 (50) 416 (50)	Vrankovic et al 2016[133]
Si/C/ SiOC (18)	1100	2000		(100)	Vrankovic et al 2016[134]
Si/ SiOC-0.6 (100)	800	980	37	800 (100)(100) 600 (100)(500) 480 (500)\(500)	Wu et al 2019 [135]
Si- SiOC S-1 ()	-	2000	28	1750 (100)	Wei et al 2020[136]
Sn/SiOC composites					
$SiOC_{MK}$ /Sn (37) $SiOC_{RD}$ /Sn (37)	1000	566 651	52 36	232 (110) 562 (110)	Kaspar et al 2014[137]
0.1 Sn- SiOCfiber 1200(35) 0.2 Sn- SiOC fibe1200 (35)	1200	939 994	18 16	457 (100) 400 (100)	Tolosa et al 2018[126]
SiOC/Sn-40 (18.6)	1000	756	26	549 (50)	Dubey et al 2019[123]
Sn@SiOC (100)	700	800	30	502 (300)	Shi et al 2019[138]

Sn@SiOC NPs (186)	900	656	33	411 (250)	Xia et al 2020[139]
Sn@SiOCNP (100)	600	918	27	~708 (200)	Wang et al[140]
SiOC:C$_{0.2}$/Sn-40% (100) SiOC:C$_{0.2}$/Sn-60% (100) SiOC:C$_{0.1}$/Sn-60% (100) SiOC/Sn-40% (100)	1000	439 507 512 572	44 38 37 35	351 (100) 441 (100) 378 (100) 521 (100)	Knozowski et al 2022[124]
SiOC- SiO$_2$ hybrid spheres (100) Bulk SiOC (100) SiOC spheres (100)	900	525 533 880	42 54 42	319 (100) 235 (100) 804 (100)	Shi et al 2017[60]
Other (Sb,BNNT,MnO,MoSe)/SiOC composites					
SiOC/Sb (18.6)	1000	667	41	507 (200) (372)	Dubey et al 2020[127]
SiOC–BNNT-0.25 wt% (100) SiOC–BNNT-0.5 wt% (100) SiOC–BNNT-2 wt% (100)	1000	410 250 317	50 58 54	237 (25) (1.6 A/g) 47 (25) (1.6 A/g) 82 (25) (1.6 A/g)	Abbas et al 2017[141]
C/ MnO/SiOC (100) MnO/SiOC (100)	500	714 737	39 39	770 (200) 600 (200)	Huang et al 2019[142]
SiOC/MoSe$_2$fiber mats	800	586	42	400 (100) (50 mA/g)	Dey et al[129]

6.2. Enhancing the network connectivity between SiOC particles

The lack of an interconnected network between SiOC particles is a significant hurdle in fabricating these anode materials. By doping SiOC nanoparticles with boron, Zhu and co-workers demonstrated that an interconnected network of nanoparticles can be formed [143]. The boron acid coating on SiOC initially transforms to solid boron oxide at elevated temperatures. Subsequent thermal treatment beyond its glass transition temperature leads to the melting of boron oxide, which will penetrate the SiO$_x$ species forming a strong interfacial bonding. The robust coupling achieved because of this boron doping has enabled the fabrication of batteries with long life and high specific capacity at high current densities [143]. The schematic illustration of the assembly formation in B doped SiOC is illustrated in Figure 5. Furthermore, the addition of boron nitride nanotubes (BNNTs) could affect the free carbon evolution, which would result in improved electrochemical performance [141]. Adding 0.25 wt% BNNT resulted in a first-cycle storage capacity of 812 mAh/g, which decreased with increasing BNNT weight fraction.

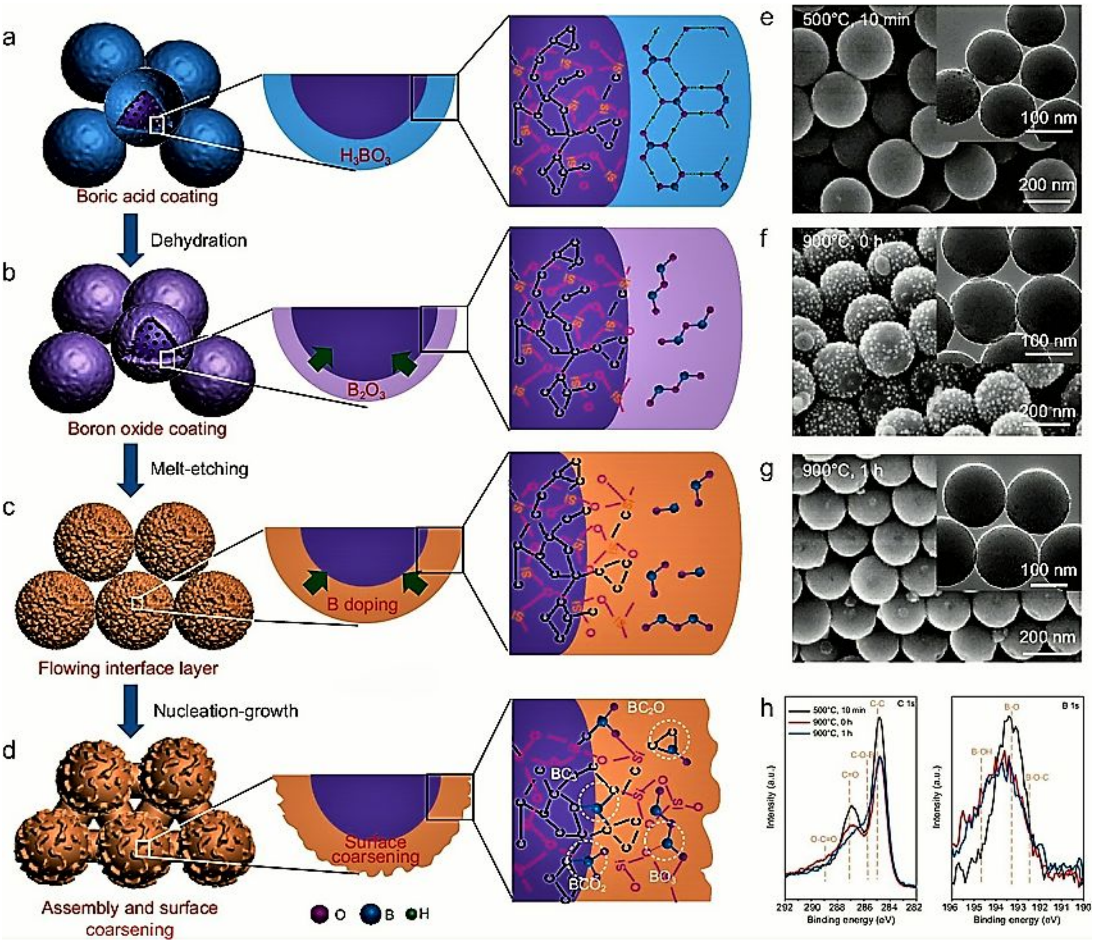

Fig. 5 (a–d) Schematic illustration of the assembly formation. (e–g) FESEM images of B-SiOC-2 at different reaction stages, and insets are corresponding TEM images. (h) C 1s and B 1s regions of the high-resolution XPS spectra of the B-SiOC-2 at different reaction stages[143]. Reproduced with permission from ref. 143. Copyright 2020, Oxford University Press.

6.3 Introducing micropores in the ceramic matrix

The PDC route produces these ceramics, which are inherently porous due to the evolution of organic species. The porous anodes may not provide the best-performing anodes since porosity inherently reduces active material, leading to low energy densities. However, pores, especially microsized ones, enhance the structural stability of these anodes due to their buffering capacity. Further, it is also being observed that nanopores could ensure faster ion diffusion to the active sites of SiOC and provide more electrochemically active sites for lithium storage [29,82]. Such structural changes have resulted in high specific capacities of 980 mAh/g at a current density of 180 mAh/g [82]. In these systems, such high porosity levels and specific surface areas can be attained by etching with either KOH or HF [62,63]. However, excessive etching could also degrade battery performance [63]. By etching with HF, for instance, the Si-O active sites will be removed from the system, resulting in poor battery performance.

In order to overcome etching issues, SiOC can be embedded in porous carbonaceous networks. Zhiyuan and co-workers infiltrated graphene sponge with SiOC precursor and subsequently pyrolysed them to produce a hierarchical 3D interconnected structure of SiOCnanolayers wrapped in graphene sponge. Designing such hierarchical structures demonstrated improved electrical conductivity and ionic diffusivity [117]. In a similar study, Gaofeng and co-workers have also shown that fabricating graphene aerogel/SiOC heterostructures can improve the battery performance compared to unsupported silicon oxycarbide. They achieved a stable reversible charge capacity of 751 mAh/g with Coulombic efficiency of ~ 99% after the first cycle [118].

6.4 Fabricating thin film SiOC anodes

Thin films of SiOC are reported to perform better than bulk counterparts [105,143]. At very high C rates, these thin-film SiOC anodes exhibited a reversible storage capacity of 1000 mAh/g. Thin films of these ceramics were fabricated by spray depositing the polymeric precursor on the Cu, and then they were converted to ceramic by pyrolysing it at 1000°C. However, they have noticed that beyond a thickness of 1 µm these films get peeled out of the Cu substrate due to the volumetric changes occurring during the lithium cycling [143]. In another study by Wei and co-workers, thin film anodes of Si/SiCO exhibiting reversible capacities of 2000 mAh/g were reported [136]. They achieved such exceptional recharge capacities due to the presence of nanosilicon. First principle studies on such systems revealed that the small size voids, less than 1 nm, present in Si-C/O tetrahedrons create a suitable environment for lithium-ion insertion [136].

6.5 Synthesizing SiOC anodes with spherical morphology

In another exciting strategy, SiOC with spherical morphology has been synthesized in order to improve the performance of anodes [2,60,93]. Such systems have shown a stable reversible capacity of ~ 900 mAh/g at a current density of 100 mA/g with a Coulombic efficiency of ~98% [60]. These SiOC spheres are typically synthesised by a sol-gel process followed by carbonisation in the Ar atmosphere. Other methods, such as emulsion templating, were also utilized to synthesize spherical SiOC microbeads with hard and dense surfaces [2]. The porous interior structures of these microbeads could also account for the faster diffusivity of Li-ions (4.5×10^{-6} cm^2/s) and eventually lead to better performance. Interestingly, such systems exhibited a high first-cycle Coulombic efficiency of ~ 73% compared to other SiOC systems (~ 50% or less) [93].

6.6 Modifying the synthesis route

Several alternative processing strategies have been reported for synthesising SiOC ceramics, and the processing parameters significantly affect battery performance. One such technique involves mixing silicon tetraacetate with citric acid and thermally treating it at 250 °C. Subsequently, the solid material is carbonised in the Ar atmosphere. Detailed characterisation using X-ray photoelectron spectroscopy revealed the presence of oxycarbide species. The galvanostatic charge/discharge experiments on such systems showed a capacity of 590 mAh/g at 50 mA/g. Further, in this study, a prelithiation step has been carried out to improve the reversible capacity [97]. Benjamin and co-workers demonstrated the significance of choosing a continuous microjet reactor technique for producing large quantities of SiOC (Figure 6). In this study, different types of alkoxysilanes were attempted. Among those, a mixture of vinyl and phenyltrimethoxysilane was identified as the best-performing material with a reversible storage capacity of 922 mAh/g [4].

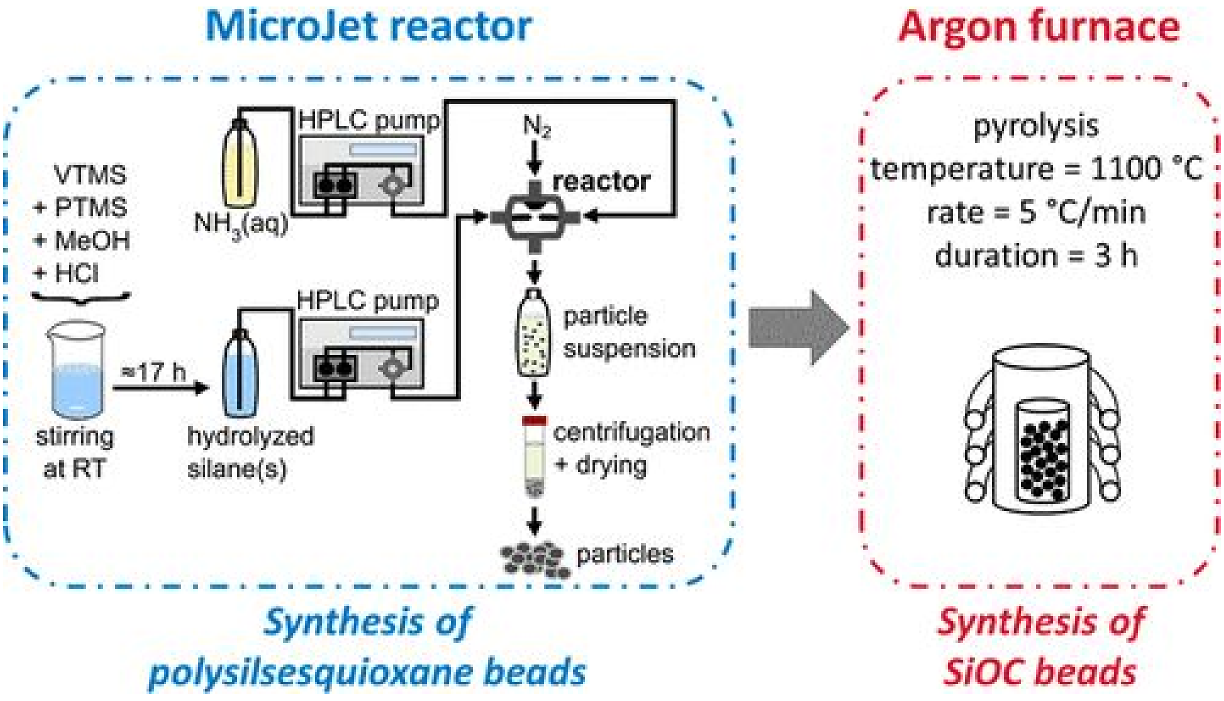

Fig. 6 Schematic synthesis using the MicroJet reactor to obtain polysilsesquioxane beads transformed to silicon oxycarbide beads via thermal treatment in argon[4,144].Reproduced with permission from ref. 144. Copyright 2018, American Chemical Society.

6.7 Prelithiation

The low initial Coulombic efficiency (ICE) is one of the major constraints that limit its practical application of SiOC [60,68,117]. To overcome the challenge of lower ICE, several prelithiation strategies have been proposed in the literature, including electrochemical prelithiation, chemical prelithiation, and doping prelithiation agents [145,146]. Among these techniques, the electrochemical prelithiation technique is widely employed, but scaling it for applications is a challenge [147]. X. Lin and co-workers have proposed an in-situ chemical prelithiation technique by injection pyrolysis of lithium hepta(i-butyl) silsesquioxanetrisilanolate to produce cells of high ICE [35]. Li_xSiO_y will be formed in situ during the pyrolysis of the precursor, thereby reducing the consumption of Li-ions in the initial cycles leading to high ICE. Further, the onion-like structure formed during the synthesis is capable of buffering the large volumetric strains during repeated cycling (Figure 7).

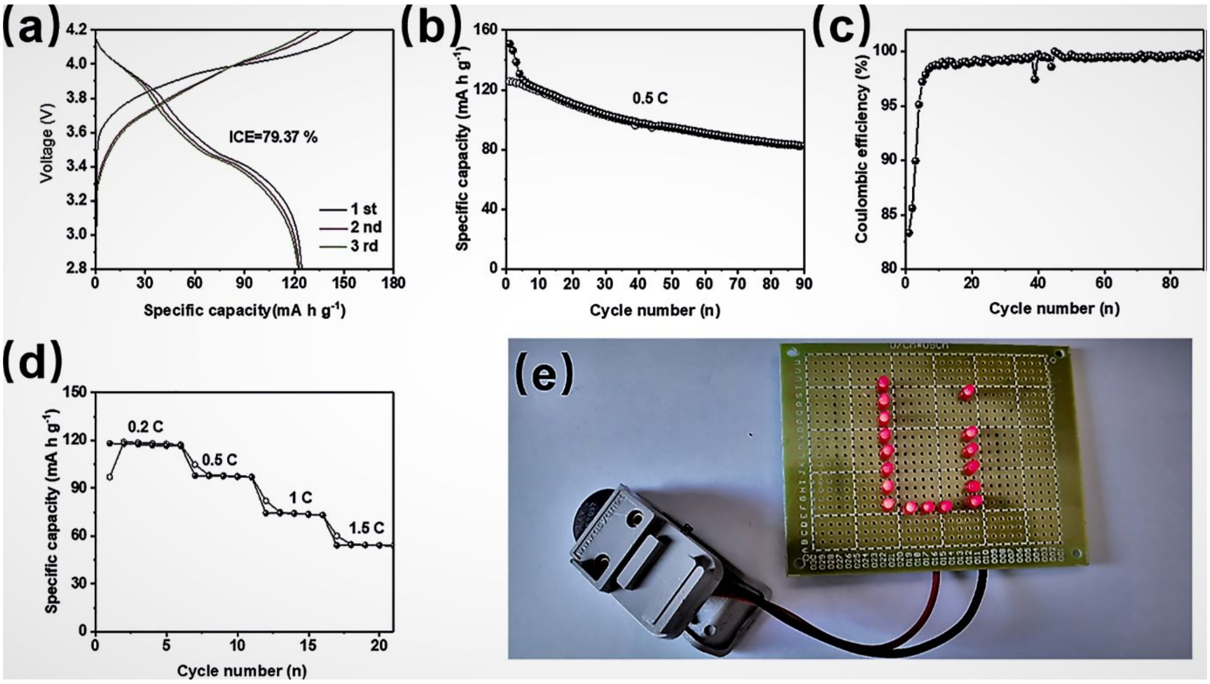

Fig. 7 (a) Voltage profiles for the first three cycles at 0.4 C, (b) cycling performance, (c) coulombic efficiency at 0.5 C, and (d) rate performance of as-assembled (−)pre-SiOC/C||LCO(+) full cell, and (e) the digital image of LED bulb array lit up by as-assembled (−)pre-SiOC/C||LCO(+) full cell[35]. Reproduced with permission from ref. 35. Copyright 2020, Elsevier.

6.8 Bio-templating method

In another novel strategy for the synthesis of SiOC ceramics, microalgae-based on Nannochlropsis [148] and Chlorella [142] were used as bio-templates (Figure 8). In another interesting study, rose pollens were considered the bio-template and carbon source

[99]. Further, supercritical CO_2 fluid was used as the solvent since these were found to ensure efficient mass transfer and uniform dispersion of precursors. By following this route, Xia and co-workers could produce SiC_nO_{4-n} species embedded in an amorphous carbonaceous network, thereby enabling a reversible charge capacity of 450 mAh/g at a current density of 0.1 A/g with an excellent Coulombic efficiency of ~ 100% [149]. In the chlorella-based system, Hui and co-workers demonstrated that by embedding MnO nanoparticles in the SiOC matrix, a stable reversible capacity of 770 mAh/g at 100 mA/g can be achieved [142]. These studies suggest that it is possible to achieve high storage and cycle retention capabilities by tailoring the morphologies and microstructures of SiOC.

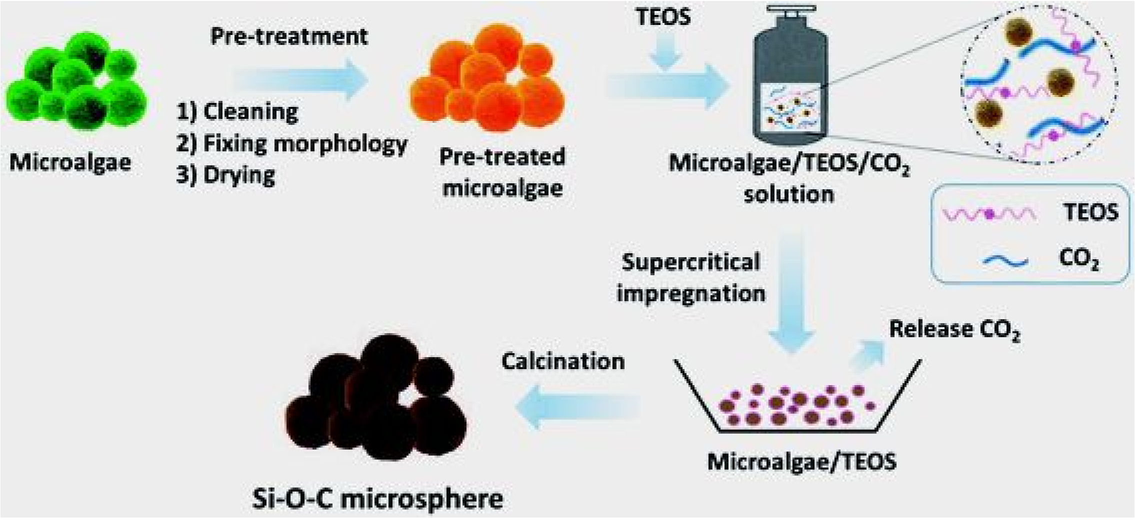

Fig. 8 Schematic illustration of the preparation process of SiOC microspheres based on bio-templating methods with the assistance of supercritical CO_2 fluid [149]. Reproduced with permission from ref. 149. Copyright 2016, Royal Society of Chemistry.

7. Mechanical properties

The SiOC based anode materials are rarely examined for their mechanical properties in the literature. From our literature survey we can find only one study in which uniaxial tensile tests were conducted on paper electrodes embedded with SiOC in a reduced graphene oxide matrix [121]. They used custom-built equipment to perform the uniaxial tensile tests (Figure 9.a-e). The reduced graphene oxide sample exhibited a strength of ~10.7 MPa at a failure strain of 2.8%, whereas the silicon oxycarbide (60 wt.%) embedded reduced graphene oxide sample exhibited a tensile strength of ~2.7 MPa at a failure strain of 1.1%. The reported strains to failure are significantly large, indicating that the anodes can accommodate enormous volumetric strains. Further, they noticed the presence of microfeatures on the surface of the anode after the tensile test. Interestingly, the fracture modes in reduced graphene oxide paper and the composite paper differed distinctly. The reduced graphene oxide paper has suddenly failed with a crumpled crack surface. Whereas the cracked surface was sharp in the composite paper [121].

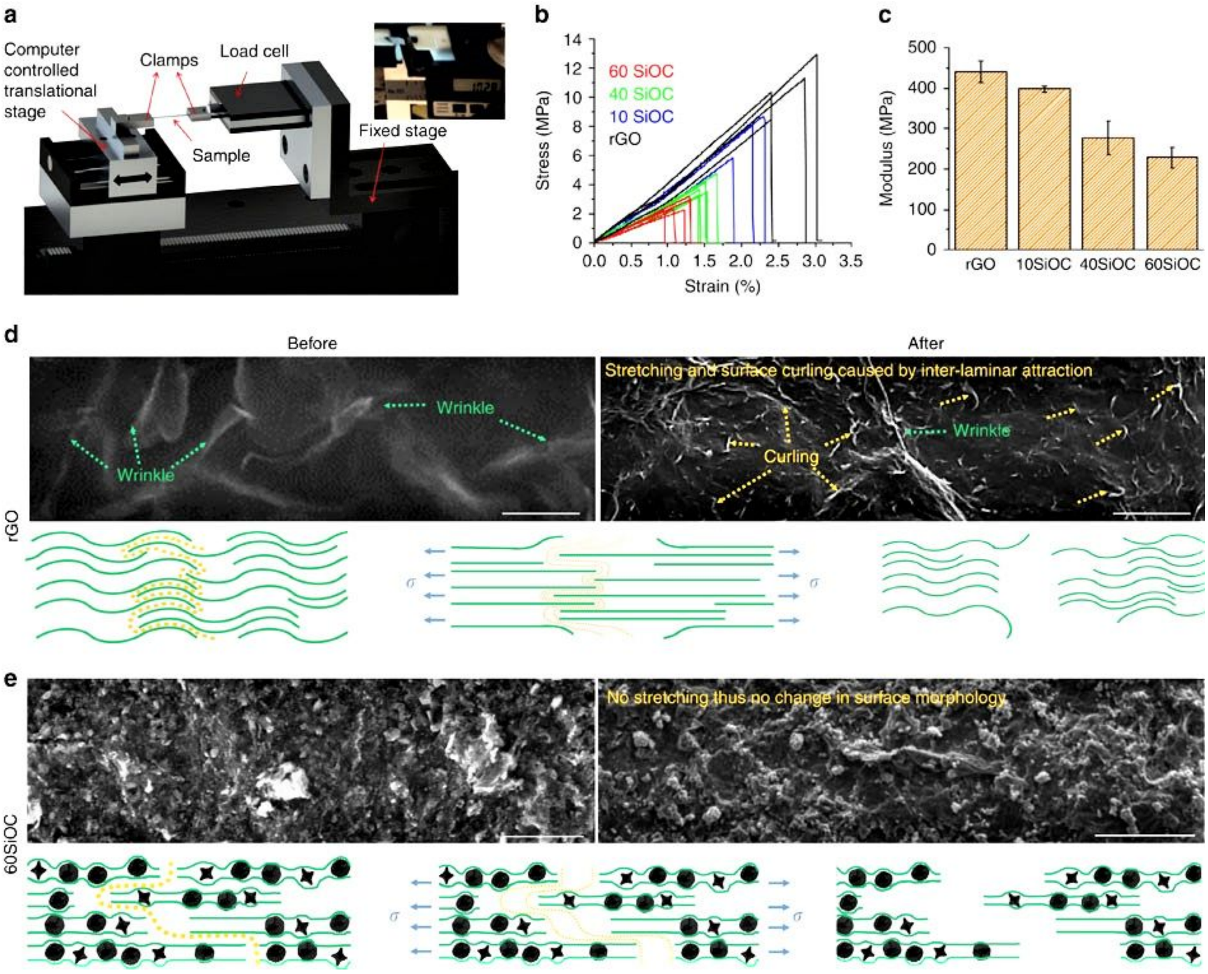

Fig. 9(a) Schematic of the tensile testing setup with a photograph of rGO paper immediately after the fracture. Scale reading in the photograph indicates the length change to be ~0.28 mm. (b) Engineering stress versus strain plots of various freestanding papers derived from load versus displacement data, and (c) their corresponding modulus values. Error bars are 26.8, 7.6, 41.5, 24.1 MPa for rGO, 10SiOC, 40SiOC, and 60SiOC, respectively. The SEM images and schematic illustration show the predicted fracture mechanism in rGO and 60SiOC freestanding papers: (d) The rGO paper experienced stretching and rearrangement of graphene sheets before failure. (e) For 60SiOC paper, negligible stretching or rearrangement occurred. The fracture line follows SiOC particles embedded in rGO flakes, resulting in gradual separation/tearing of the paper. The scale bar is 20 µm in all images[121].Reproduced with permission from ref. 121. Copyright 2016, Springer Nature.

8. Other electrochemical applications

8.1 Enhancing the electrochemical performance of Si-anodes

Silicon has a very high theoretical capacity of (~ 4200 mAh/g), ~ 10 times that of graphite. However, as discussed above, due to high volumetric expansion (~ 300%), it is challenging to envisage Si as an effective anode material. One way to overcome this constraint is to synthesize silicon particles embedded in SiOC matrix [100,130,132]. By embedding Si nanoparticles with an amorphous SiOC matrix, the extreme volumetric strains experienced by the silicon particles can be suppressed, and the free carbon present in the matrix can act as a good electrical conductor. One method by which it is synthesised is the selective assembly method, and by effectively using surfactants such as cetrimonium bromide (CTAB), interfacial interactions between silicon nanoparticles and silicon oil can be ensured. Such studies have shown a stable capacity of 1312 mAh/g for 100 cycles at 0.5 A/g (Figure 10) [100].

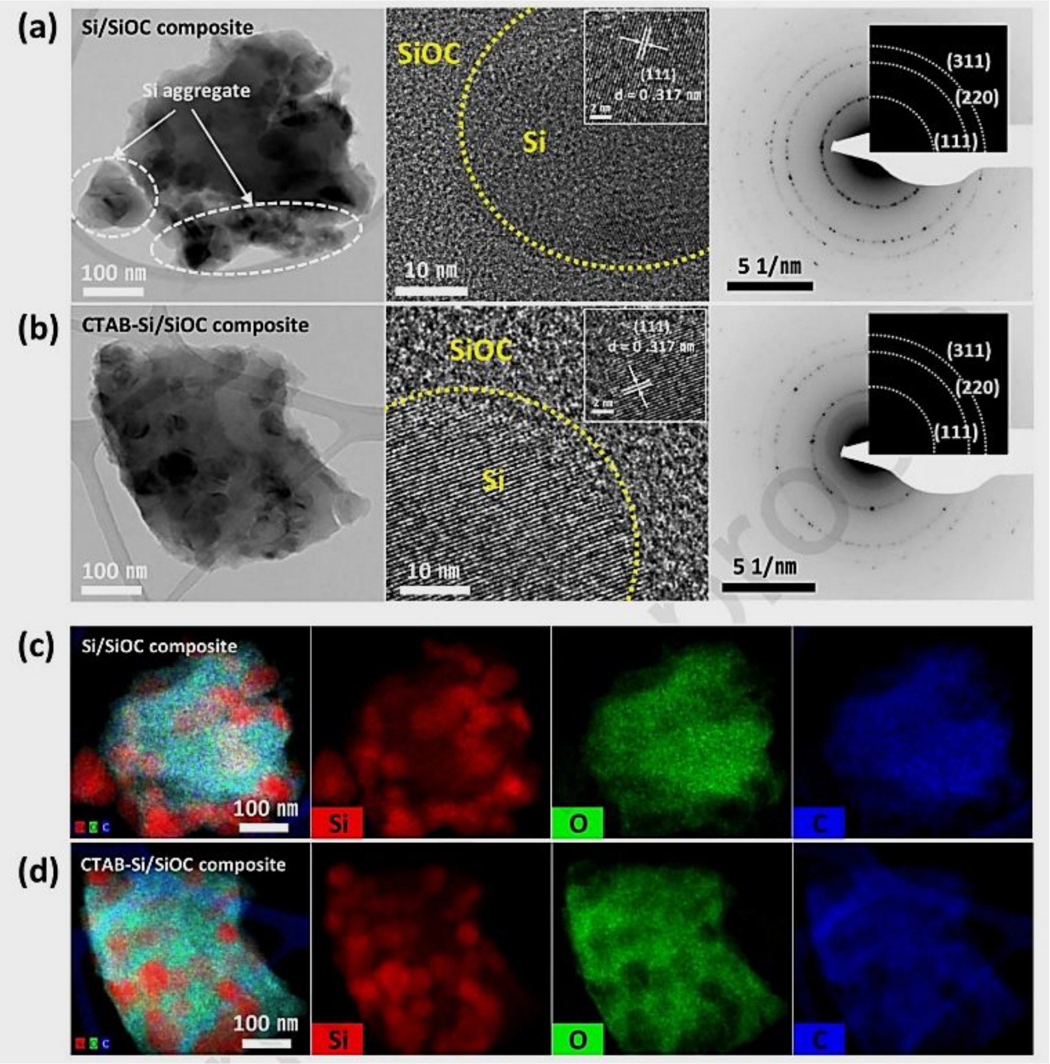

Fig. 10 Low-magnified TEM images, HR-TEM images with inset showing the lattice fringes of the Si, and SAED patterns of (a) Si/SiOC and (b) CTAB-Si/SiOC composite. EDS mapping of (c) Si/SiOC and (d) CTAB-Si/SiOC composites including elemental Si, O, and C[100]. Reproduced with permission from ref. 100, Copyright 2020, Elsevier.

In another method, Si nanoparticleswere coated with suitable polymeric precursors, and then pyrolysed to synthesise SiOC-embedded Si particles. These SiOC-embedded systems resulted in the fabrication of fracture-free silicon anodes having a reversible capacity of 2093 mAh/g with a Coulombic efficiency of 92% after 200 cycles [132]. Their transmission electron microscopy studies reveal that the silicon oxycarbide-coated Si anodes are more robust than traditional graphite-coated Si anodes. This study has achieved the coating by a scalable spray pyrolysis process. The coating was stable since the SiOC glass phase can expand during the lithiation and therefore accommodate the volumetric strains of the inner silicon nanoparticle. Furthermore, the SiOC phases act as a bridge between silicon nanoparticles, thereby improving structural integrity. However, the optimum thickness required to achieve the required capacity has not been discussed in this study.

8.2 Lithium-tin anodes

SiOC materials were also explored to improve the structural integrity of lithium-tin anodes. A tin-based anode has a reversible storage capacity of 994 mAh/g, which is about three times higher than a graphite anode [14]. However, similar to Si anodes, these materials expand significantly (~260%) during lithiation, thereby leading to poor structural integrity. Several efforts toward developing stable Sn anodes resulted in the development of Sn anodes dispersed in the SiOC matrix. Kaspar and group synthesised SiOC/Sn nanocomposites by chemically modifying the polysiloxane precursors (C-rich and C-lean) with tin acetate [137]. The Sn nanoparticles were 10 to 45 nm in size. Their studies revealed a first-cycle storage capacity of 651 mAh/g for the C-rich precursor-based system. They hypothesised that the excess C present in these systems is responsible for accommodating the volumetric strains, thereby leading to better structural integrity. Further, they have also observed a dependency of the type of Li-Sn alloy formation on the composition of the SiOC. In the C-rich system, Li_7Sn_2 was observed, whereas for the C-lean system, $Li_{22}Sn_5$ was observed. However, achieving homogeneous distribution of Sn nanoparticles in the matrix was difficult in these systems leading to relatively lower cyclic stability. The presence of highly ordered C further limited its reversible storage capacities. Hence, Dubey and co-workers synthesised SiOC/Sn nanocomposites to overcome these challenges by chemically modifying polysiloxaneprecursors with tin ethyl hexanoate

[123]. By choosing tin ethyl hexanoate instead of tin acetate, they could achieve better homogeneity in the matrix. Moreover, the excess carbon observed in these new systems was highly disordered yielding storage capacities of 553 mAh/g at a current density of 2232 mAh/g. Further, the scanning transmission electron microscopy studies of the samples that are cycled after 180 cycles revealed insignificant pulverisation, demonstrating the high structural stability of these composite systems [123].

8.3 Sodium-ion batteries

In light of the wide availability of sodium, rechargeable sodium-ion batteries are considered an alternative to lithium-ion batteries. However, sodium ions have a much larger size than lithium ions, resulting in severe volumetric fluctuations during charging and discharging. The density of sodium is higher (0.97 gm/cm$^{3)}$ than the Li-ions (0.53 gm/cm^3) which make it heavier. The ionic radius of Na-ion is also much larger than that of Li-ion which may lead to low packing density and severe volumetric strains. Therefore, the efforts are towards developing suitable anode materials to accommodate sizeable volumetric strain. Several studies have shown that 2D materials such as $MoS_{2,}$ because of its large inter-layer spacing of 0.62 nm, can act as a good host for sodium ions [150–152]. However, due to its low electrical conductivity and structural instability, capacity fading seems severe in MoS_2-based systems. H. Lim and co-workers have shown that by encapsulating MoS_2 in SiOC, it is possible to improve the structural stability of MoS_2.Further, to improve the electrical conductivity, they have done nitrogen doping of MoS_2. Their studies show that these core-shell structures can result in high storage capacities of 540.7 mAh/g with a capacity retention of more than 100 cycles [153]. Similar to MoS_2, antimony is also a suitable candidate anode material for sodium-ion batteries. It has a theoretical capacity of (660 mAh/g). However, its practical utility is limited because of its high volumetric expansion and sluggish kinetics. Hence, like MoS_2, Lee and co-workers embedded Sb in a silicon oxycarbide matrix and demonstrated a storage capacity of 510 mAh/g. Moreover, the capacity is retained for 250 cycles at 97% efficiency, even at a high current density of 20 C [154]. These studies show that encapsulating the active material in an amorphous SiOC can improve the structural stability of these anode materials.

Interestingly, SiOC synthesised from silicone oils was also directly explored as an anode material in sodium-ion batteries. Their cell capacities were somewhat limited to 160 mAh/g at 25 mA/g for 200 cycles. Nevertheless, the stability of such systems was exceedingly high - 00.09 mAh/g decay per cycle for 650 cycles [155]. Since the overall capacities are very low, strategies such as increasing the amount of carbon-rich SiOC phases and decreasing the presence of inactive sites such as SiO_2, SiC and free carbon phases were explored by other researchers [156]. Moreover, detailed structural studies using X-ray photoelectron and nuclear magnetic resonance spectroscopy have revealed interesting results in these systems [157]. They have selected two techniques for the analysis, one etched with HF having considerably high porosity levels and the other unetched. Comparison between the two indicated that SiOC acts as active sites for sodium, but the mechanism seems to be not an alloying mechanism. Instead, due to the initial sodium intake, an irreversible structural change occurs,contributing to sodium intake. Further, systematic studies toward understanding the mechanism of sodium intake in SiOC ceramics were carried out with ex-situ measurements and DFT calculations [158]. Based on the various ex-situ analyses, they concluded that sodiation up to 0.4 V occurs mainly in the carbon-rich SiOC phase and the micropores, whereas at voltages between 0.4 - 0.1 V, silicon-rich sites were activated for sodiation. However, at voltages below 0.1 V, sodium ions tend to react with amorphous Si to form silicon-rich compounds. Interestingly, SiC sites seem to contribute significantly to the cycling stability up to 6000 cycles at 200 mA/g [158]. The details of the electrochemical performance studies on sodium-ion batteries employing SiOC and SiOC-based composites as anodes are presented in table 5.

Table 5 The Electrochemical performance of sodium-ion batteries employingpolymer derived SiOC and various SiOC-based composites as anodes.

Specimen (current density mA/g)	Synthesis temperature (°C)	First reversible capacity (mAh/g)	First cycle loss (%)	Reversible capacity (mAh/g) (after N cycles) (Current density (mA/g)	Reference
SiCO_Ph (25) SiCO_Ph_T (25)	1000	83 188	70 53	- 150 (40)	Weinberger et al (93)
SiOC/HC_G (37)	1000	201	35	141 (50)	Kaspar et al [159]
SiOC(N)/HC_G(37)	1000	110	49	105 (50)	Kaspar et al [159]
SiOC /HC_{PS}(37)	1000	140	45	67(50)	Kaspar et al [159]
SiOC(N)/ HC_{PS}(37)	1000	56	67	42 (50)	Kaspar et al [159]
Sb/SiOC (18.6)	900	510	32.4	480 (250) (74)	Lee et al [154]
900C-1h-10M (25)	900	189	57	160 (200)	Chandra et al[155]
SiOC (20)	1000	175	63	100 (500)	Dou et al[157]
SiOC- (BPO-C) (50)	1000	226	62	166 (10) decreased drastically after 90 cycles	Weinberger et al[29]
SiOC-1300 (25)	1300	210	70	125 (600)	Chandra et al[158]
HFC- Sb/SiOC (33) LFC- Sb/SiOC (33)	900 900	403 376	34.5 34.5	344.5 (150) (0.2-C) 217 (150) (0.2-C)	Kim et al[128]
SIOC with FEC (25) SIOC without FEC (25)	900 900	226 (10) 184 (10)	54 60	191.7 (20) -	Putra et al[160]
MoS_2–SiOC (25)	800	199	30	190 (100)	Marcelo et al[152]
N-MoS2/ C@SiOC	900	540.7	24.5	~692(200)	Lim et al[153]

SiOC (DS-N2-1) (25)	900 then 1300	234	41.5	160 (140)	Chandra et al[156]
HC-SIOC-1(50)	1200	295	34	260 (50)	Cheng et al[161]

8.4 Supercapacitors

Supercapacitors fabricated out of SiOC ceramics were also investigated. Using electrospinning and pyrolysis, SiOC fibre mats were prepared from three preceramic polymers (MK, H44, and RSN) and evaluated for specific capacitance. Due to the higher concentration of free carbon in H44 (methyl-siloxane), electrodes prepared from this material showed the best performance with a specific capacitance of 50 F/g and capacity retention of 100% for 2000 cycles [98]. Moreover, NiO loaded on Ni-S doped silicon oxycarbide (NSCDC) exhibited excellent cyclic properties and exhibited a capacitance of 804 F/g at 1 A/g. It was achieved by NSCDC's excellent electrical conductivity and its hierarchical porous structure, which enhanced ionic and electronic transport [162]. Surprisingly, an ultra-low carbon-SiOC ceramic synthesized by pyrolyzing a silicone oil rich in phenyl was found to be effective for LIB because of its low reversible storage capacity (238 mAh/g). This exhibited pseudocapacitor properties at a voltage range of 0-1 V versus Li/Li^+ [163]. The electrochemical performance details of SiOC material employed as supercapacitor in the literure are tabulated in table 6.

Table 6 The electrochemical performance of SiOC materials employed as supercapacitor.

Specimen & (Current density)	Synthesis temperature	Capacitance (F/g)	Electrolyte	Specific surface area (m^2/g)	Capacity retention % (no of cycles)	Reference
SiOCDC-1 (30 A /g)	1000	110	1 M TEABF4 in acetonitrile	~2000	95% (10,000)	Meier et al 2014[164]
SiOC-DC (1 A /g)	1000	148.7	5 M KOH aqueous solution	2635	94.3% (2000)	Liqun et al 2015[165]
SiOC-CDC (0.1 A /g)	1200	135	1M tetraethylammonium tetrafluoroborate in acetonitrile	2394	86% (10000)	Tolosa et al 2016[166]
SiOC (4.5 A /g)	900	-	1 M $LiPF_6$ a 1:1:1 v/v mixture of EC/ DMC/EMC	3.2	90% (75000)	Halim et al 2017[163]
LBL-SiOC-rGO (6.7 A /g)	800	75.72	6M KOH aqueous solution	-	56.13 (464)	Kothadi et al[112]
SiOC 0.5 wt% BNNT(1 A /g)	1000	78.93	6M KOH aqueous solution	-	86% (185)	Abbas et al 2017[141]
SiOC SSCs (5 mV/s)	900	141 115	1 M Li_2SO_4 1 M $TEABF_4$	5.64	86.2 92.8 (5000)	Pazhamalai et al 2020[167]
SiOC H44 fibers SiOCmkfibers SiOCRSNfibers (100 mV/s)	1000	50 30 20	1M aq. Na_2SO_4	278.2	100 (2000)	Mujib et al 2020[98]

NSDC NiO-10 (1 A/g)	300	804	3 M KOH	899	73.2 (5000)	Pan et al 2021[162]
SiC/SiOC/ C (1mA/ cm^2)	1500	27.2 mF/cm^2	2 M KCl	-	90 (1000)	Okoroanyanmu et al 202[168]
TPTS SiOC (2 mV/s)	800	78 (474 mF/cm^2)	1 M H_2SO_4	235	100 (5000)	Mujib et al 2021[96]
NHXF (20 mV/s)	1000	333	6 M KOH	1798	-	Swain et al 2022[169]
TRP13F24 (0.1 A/g)	1300-1400	225-165	1 M H_2SO_4	550	-	Mazo et al 2022[170]

9. Summary and Perspectives

The use of PDC-based materials is expected to have a significant impact on the development of high-capacity, energy-efficient batteries and supercapacitors. Hence, as we have seen through this review silicon oxycarbides as anode materials in lithium ion batteries is widely explored. Due to their amorphous and porous nature, they have an electrochemical storage capacity almost double that of graphite anodes. As discussed in this review, we have highlighted the various factors that affect electrochemical performance, the significance of first-principle studies, as well as strategies for overcoming the inherent challenges.

In spite of recent progress, there are still scientific issues to be resolved to ensure its commercial viability. Identifying a precursor that would provide the best electrochemical performance is one of the major challenges. For the synthesis of SiOC anodes, several types of precursors have been reported in the literature. These factors result in a wide range of energy storage values from 200 to 1300 mAh/g. A number of SiOC ceramics have high storage capacities, but they tend to be poor cyclable anodes. In some other systems, however, the reverse is true. It is therefore essential to have a deeper understanding of precursor chemistry in order to fabricate cells that are capable of meeting the demands of industrial applications. We suggest implementing a standardized synthesis procedure for SiOCs to ensure better repeatability. Furthermore, it is important to ensure the proper selection of precursors that guarantee a ceramic yield of more than 90% to ensure its commercial viability. Furthermore, a higher yield not only ensures low volatile emission but also enhances the environmental friendliness of the synthesis procedure.

To gain deeper insights into mechanisms causing irreversibility and fade in SiOC systems, invasive characterisation techniques should be used after cycling or after lithiation. A combination of first principle and computational studies as well as machine learning techniques may be applied to determine the best precursor chemistry. Electrochemical characterisation studies should be conducted according to standard testing protocols to assess cell performance, such as current density, C-rate, rate capability, etc., so that proper comparisons between different SiOC systems can be made.

In contrast to Si-anodes that are widely researched, SiOC anodes and their interactions with various other cell components such as current collectors, electrolytes, and binders are less well explored and understood. A number of additives have been explored, and graphene is one of the most prominent. Research should be conducted to develop conductive binders and additives for electrolytes in order to increase the energy density of these batteries. For practical applications, it is crucial to have a homogeneous distribution of PDC material in the electrode. In addition, the role of particle size and distribution on electrochemical properties is unclear. According to previous studies, the interface between the SiOC electrode and the Cu current collector is improper, which results in inefficient energy transfer. The use of alternative current collectors such as Bucky papers could ensure a proper interface[171]. Further, the fabrication of these anodes should take advantage of advances in recent fabrication techniques, including lithography and additive manufacturing. The mechanical stability and safety of the device is another aspect that is crucial for determining its suitability for practical applications. As far as we know, there has not been a detailed study on this topic. Despite SiOC anodes' advantages over counterparts such as Si and graphite anodes, it is still a long way from commercial viability for large-scale applications.

Conflicts of interest

Authors declare that they do not have any conflicts of interest.

Acknowledgements

Authors would like to acknowledge HBL Power Systems Limited for funding the project related to Li-ion Batteries and providing access to various research facilities in their R&D lab. This work was partially supported by the US National Science Foundation EPSCoR Program under NSF Award # OIA-1655740. The US National Science Foundation Graduate Research Fellowship Program GRFP (DGE-1744593) also provided additional support for Michelle Greenough. However, the views, conclusions and recommendations expressed in this material are those of the author(s) and do not necessarily reflect those of the US National Science Foundation.

Authors Biographical Sketch

Ravindran Sujith : *Sujith is currently working as an Associate Professor in the Mechanical Engineering Department at BITS Pilani Hyderabad Campus. He received his B. Tech from Kerala University, M. Tech from NIT Calicut (Gold medalist) and PhD Degree from Indian Institute of Technology Madras. He received the Early Career Research Award in 2016 from Department of Science and Technology, Govt. of India for pursuing research in the development of hydrogen storage materials. His research is mainly focused towards developing materials for energy storage applications, mechanical deformation behavior of metals and composites, theoretical studies involving DFT etc. He has contributed to more than 45 international journals publications and 2 book chapters.*

Jella Gangadhar: *Gangadhar obtained his B. Tech and M.tech degree from NCET and GRIET, affiliated to Jawaharlal Nehru technological university Hyderabad (JNTUH). He obtained his PhD degree from Birla Institute of Technology and Sciences - Pilani Hyderabad campus under the supervision of Prof. Ravindran Sujith and Co-supervision of Prof Rajendra K. Bordia of Clemson University. His research interests include development of high energy density anode materials for Li-ion batteries and the specific focus on the materials which include polymer derived Silicon oxycarbide,silicon, silicon derived from rice husk and graphene-based composites. He has authored around 7 peer-reviewed journal publications, 10 international conferences and a book chapter.*

Michelle Greenough:*Michelle Greenough with a B.S. in Chemistry and minors in Biology and Mathematics from Wagner College, NY. In 2015, she joined Prof. Bordia's group at Clemson University, pursuing her PhD. She was a recipient of the National Science Foundation (NSF) Graduate Research Fellowship in 2016. She also* *received the NSF INTERN Fellowship which she used to conduct research in France and Germany. And was a recipient of the Materials Science Department's Gilbert Robinson Memorial Fellowship. She completed her PhD in August 2021 and is currently a staff scientist at the Lawrence Livermore National Laboratories.*

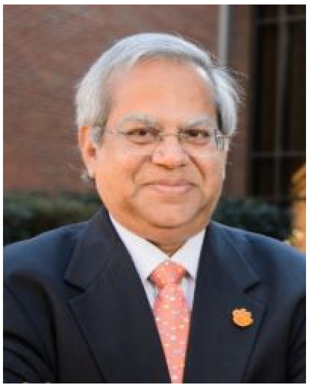

Rajendra K. Bordia: *Bordia is currently the George J. Bishop, III Professor of Ceramic and Materials Engineering in the Department of Materials Science and Engineering at Clemson University in Clemson, SC, USA. He was a faculty member at the University of Washington (1991-2013) and a Research Scientist in DuPont Co. (1986 to 1991). He received his B. Tech from IIT, Kanpur, India (1979), and his M.S. (1981) and Ph.D. (1986) from Cornell University, Ithaca, NY, USA. His research is at the intersection of materials and mechanics and is focused on fundamental and applied studies in the processing and properties of complex material systems for energy, environmental and medical applications. He has authored or co-authored over 170 peer-reviewed technical publications.*

Dillip K. Panda*: Dr. Panda is currently working as a Research Assistant Professor in the Department of Materials Science and Engineering at Clemson University. Prior to joining Clemson University, Dillip worked at Florida State University and University of Michigan as a postdoctoral fellow. He has received his M.Sc. (Gold Medal) in chemistry from NIT-Rourkela, India. He completed his Ph.D. from the University of Wollongong in 2011 under the tutelage of Prof. Gordon G Wallace. Throughout his career this work has led to more than 30 peer-reviewed publications in various journals (e.g., JACS, Chem. Sci, ACS-Appl. Mater. Interface, ACS-Sust. Chem. Eng, J. Mat. Chem. C and Chem. Comm., etc.) and three separate book chapters. His curent research focus on approaches to high-temperature all solid-state lithium battery for electric vehicles and Li-ion batteries.*

References

1 B. Diouf and R. Pode, *Renew. Energy*, 2015, **76**, 375–380.

2 B. Dong, Y. Han, T. Wang, Z. Lei, Y. Chen, F. Wang, H. Abadikhah, S. A. Khan, L. Hao, X. Xu, R. Cao, L. Yin and S. Agathopoulos, *ACS Appl. Energy Mater.*, 2020, **3**, 10183–10191.

3 H. Li, Z. Wang, L. Chen and X. Huang, *Adv. Mater.*, 2009, **21**, 4593–4607.

4 B. Krüner, C. Odenwald, N. Jäckel, A. Tolosa, G. Kickelbick and V. Presser, *ACS Appl. Energy Mater.*, 2018, **1**, 2961–2970.

5 Md. A. Rahman, G. Song, A. I. Bhatt, Y. C. Wong and C. Wen, *Adv. Funct. Mater.*, 2016, **26**, 647–678.

6 S. Chen, L. Shen, P. A. van Aken, J. Maier and Y. Yu, *Adv. Mater.*, 2017, **29**, 1605650.

7 J. E. Entwistle, G. Beaucage and S. V. Patwardhan, *J. Mater. Chem. A*, 2020, **8**, 4938–4949.

8 C. Jiang, L. Xiang, S. Miao, L. Shi, D. Xie, J. Yan, Z. Zheng, X. Zhang and Y. Tang, *Adv. Mater.*, 2020, **32**, 1908470.

9 M. Ge, C. Cao, G. M. Biesold, C. D. Sewell, S. Hao, J. Huang, W. Zhang, Y. Lai and Z. Lin, *Adv. Mater.*, 2021, **33**, 2004577.

10 Y. Qi, G. Wang, S. Li, T. Liu, J. Qiu and H. Li, *Chem. Eng. J.*, 2020, **397**, 125380.

11 X. Zuo, J. Zhu, P. Müller-Buschbaum and Y.-J. Cheng, *Nano Energy*, 2017, **31**, 113–143.

12 B. Liang, Y. Liu and Y. Xu, *J. Power Sources*, 2014, **267**, 469–490.

13 X. Huang, B. Christopher, S. Chai, X. Xie, S. Luo, S. Liang and A. Pan, *ACS Appl. Energy Mater.*, 2021, **4**, 1677–1686.

14 W.-J. Zhang, *J. Power Sources*, 2011, **196**, 13–24.

15 M. Ashuri, Q. He and L. L. Shaw, *Nanoscale*, 2015, **8**, 74–103.

16 V. S. Pradeep, M. Graczyk-Zajac, R. Riedel and G. D. Soraru, *Electrochim. Acta*, 2014, **119**, 78–85.

17 H. Fukui, Y. Harimoto, M. Akasaka and K. Eguchi, *ACS Appl. Mater. Interfaces*, 2014, **6**, 12827–12836.

18 H. Sun and K. Zhao, *ACS Appl. Mater. Interfaces*, 2017, **9**, 35001–35009.

19 P. A. Loughney, S. B. Mujib, T. L. Pruyn, G. Singh, K. Lu and V. Doan-Nguyen, *J. Appl. Phys.*, 2022, **132**, 070901.

20 P. Colombo, G. Mera, R. Riedel and G. D. Sorarù, *J. Am. Ceram.*, 2010, **93**, 1805–1837.

21 R. Bhandavat, Z. Pei and G. Singh, *Nanomater Energy*, 2012, **1**, 324–337.

22 S. B. Mujib and G. Singh, *Int. J. Ceram. Eng. Sc.*, 2022, **4**, 4–9.

23 N. Liao, M. Zhang, B. Zheng and W. Xue, *Appl Materl Today*, 2020, **18**, 100434.

24 P. Dibandjo, M. Graczyk-Zajac, R. Riedel, V. S. Pradeep and G. D. Soraru, *J. Eur. Ceram. Soc.*, 2012, **32**, 2495–2503.

25 V. S. Pradeep, D. G. Ayana, M. Graczyk-Zajac, G. D. Soraru and R. Riedel, *Electrochim. Acta*, 2015, **157**, 41–45.

26 M. Wilamowska-Zawlocka, P. Puczkarski, Z. Grabowska, J. Kaspar, M. Graczyk-Zajac, R. Riedel and G. D. Sorarù, *RSC Adv.*, 2016, **6**, 104597–104607.

27 M. Graczyk-Zajac, L. Toma, C. Fasel and R. Riedel, *Solid State Ion.*, 2012, **225**, 522–526.

28 M. Halim, C. Hudaya, A.-Y. Kim and J. K. Lee, *J. Mater. Chem. A*, 2016, **4**, 2651–2656.

29 M. Weinberger, P.-H. Su, H. Peterlik, M. Lindén and M. Wohlfahrt-Mehrens, *Nanomater.*, 2019, **9**, 754.

30 J. Kaspar, M. Graczyk-Zajac, S. Choudhury and R. Riedel, *Electrochim. Acta*, 2016, **216**, 196–202.

31 A. Maheshwari, E. P. Gopikrishnan, J. Gangadhar and R. Sujith, *Mater. Chem. Phys.*, 2020, **239**, 121963.

32 R. Bhandavat, M. Cologna and G. Singh, *Nanomater. Energy*, 2012, **1**, 57–61.

33 L. David, R. Bhandavat, U. Barrera and G. Singh, *Nat Commun*, 2016, **7**, 10998.

34 J. Shen, *Journal of Power Sources*, 2011, 6.

35 X. Lin, Y. Dong, X. Liu, X. Chen, A. Li and H. Song, *Chem. Eng. J.,* 2022, **428**, 132125.

36 E. Ionescu, H.-J. Kleebe and R. Riedel, *Chem. Soc. Rev.*, 2012, **41**, 5032–5052.

37 W. Duan, X. Yin, Q. Li, L. Schlier, P. Greil and N. Travitzky, *J. Eur. Ceram. Soc.*, 2016, **36**, 3681–3689.

38Q. Wen, Z. Yu and R. Riedel, *Prog. Mater. Sci.*, 2020, **109**, 100623.
39G. Barroso, Q. Li, R. K. Bordia and G. Motz, *J. Mater. Chem. A*, 2019, **7**, 1936–1963.
40M. Arango-Ospina, F. Xie, I. Gonzalo-Juan, R. Riedel, E. Ionescu and A. R. Boccaccini, *Appl. Mater. Today*, 2020, **18**, 100482.
41E. Bernardo, L. Fiocco, G. Parcianello, E. Storti and P. Colombo, *Mater.*, 2014, **7**, 1927–1956.
42P. Miele†, S. Bernard, D. Cornu and B. Toury, *Soft Mater.*, 2007, **4**, 249–286.
43K. Lu, *Mater. Sci. Eng. R: Reports*, 2015, **97**, 23–49.
44S. Fu, M. Zhu and Y. Zhu, *J. Adv. Ceram.*, 2019, **8**, 457–478.
45M. Schulz, *Adv. Appl. Ceram.*, 2009, **108**, 454–460.
46R. Sujith, S. Jothi, A. Zimmermann, F. Aldinger and R. Kumar, *Int. Mate. Rev.*, 2021, **66**, 426–449.
47Q. Wen, F. Qu, Z. Yu, M. Graczyk-Zajac, X. Xiong and R. Riedel, *J Adv Ceram*, 2022, **11**, 197–246.
48 A. Viard, D. Fonblanc, D. Lopez-Ferber, M. Schmidt, A. Lale, C. Durif, M. Balestrat, F. Rossignol, M. Weinmann, R. Riedel and S. Bernard, *Adv.Eng. Mater.*, 2018, **20**, 1800360.
49 Verbeek, W. Germany Pat., DE 2218960 A1, 1972.
50G. Fritz and B. Raabe, *Z. Anorg. Allgemeine Chem.*, 1956, **286**, 149–167.
51K. Bawane, D. Erb and K. Lu, *J. Eur. Ceram. Soc.*, 2019, **39**, 2846–2854.
52C. Stabler, A. Reitz, P. Stein, B. Albert, R. Riedel and E. Ionescu, *Mater.*, 2018, **11**, 279.
53L. Wang and K. Lu, *J Mater Sci*, 2019, **54**, 6073–6087.
54R. Sujith, P. K. Chauhan, J. Gangadhar and A. Maheshwari, *Sci Rep*, 2018, **8**, 17633.
55M. Wilamowska, *Solid State Ion.*, 2014, 7.
56H. Fukui, H. Ohsuka, T. Hino and K. Kanamura, *J. Electrochem. Soc.*, 2013, **160**, A1276.
57H. Lim, H. Kim, S.-O. Kim, K. J. Kim and W. Choi, *Chem. Eng. J.*, 2021, **404**, 126581.
58G. Liu, J. Kaspar, L. M. Reinold, M. Graczyk-Zajac and R. Riedel, *Electrochimica Acta*, 2013, **106**, 101–108.
59K. J. Lee, W. Bak, J.-J. Kim, M. A. Snyder, W. C. Yoo and Y.-E. Sung, *J. Phys. Chem. C*, 2015, **119**, 7604–7613.
60H. Shi, A. Yuan and J. Xu, *J. Power Sources*, 2017, **364**, 288–298.
61B. V. Manoj Kumar and Y.-W. Kim, *Sci..Technol. .Adv. Mater.*, 2010, **11**, 044303.
62M. Ma, H. Wang, M. Niu, L. Su, X. Fan, J. Deng, Y. Zhang and X. Du, *RSC Adv.*, 2016, **6**, 43316–43321.
63K. Xia, Z. Wu, C. Xuan, W. Xiao, J. Wang and D. Wang, *Electrochim. Acta*, 2017, **245**, 287–295.
64X. Liu, M.-C. Zheng and K. Xie, *J. Power Sources*, 2011, **196**, 10667–10672.
65J. S. Xue, K. Myrtle and J. R. Dahn, *J. Electrochem. Soc.*, 1995, **142**, 2927.
66H. Fukui, H. Ohsuka, T. Hino and K. Kanamura, *ACS Appl. Mater. Interfaces*, 2010, **2**, 998–1008.
67H. Fukui, H. Ohsuka, T. Hino and K. Kanamura, *J. Electrochem. Soc.*, 2011, **158**, A550.
68H. Fukui, K. Eguchi, H. Ohsuka, T. Hino and K. Kanamura, *J. Power Sources*, 2013, **243**, 152–158.
69H. Fukui, H. Ohsuka, T. Hino and K. Kanamura, *J. Power Sources*, 2011, **196**, 371–378.
70N. Liao, B. Zheng, M. Zhang and W. Xue, *J. Mater. Chem. A*, 2016, **4**, 12328–12333.
71C. Chandra, W. Devina, H. S. Cahyadi, S. K. Kwak and J. Kim, *Chem. Eng. J..*, 2022, **428**, 131072.
72N. Liao, B. Zheng, H. Zhou and W. Xue, *J. Mater. Chem. A*, 2015, **3**, 5067–5071.
73N. Liao, B. Zheng, H. Zhou and W. Xue, *Electrochim. Acta*, 2015, **156**, 115–120.
74N. Liao, B. Zheng, H. Zhou and W. Xue, *J. Power Sources*, 2016, **334**, 39–43.
75P.Kroll, *Mater Res SoC Symp Proc,* 2011, **1313**, 7.

76N. Liao, M. Zhang, B. Zheng and W. Xue, *J. Phys. Chem. C*, 2019, **123**, 19315–19321.
77M. Graczyk-Zajac, L. Reinold, J. Kaspar, P. Sasikumar, G.-D. Soraru and R. Riedel, *Nanomater.*, 2015, **5**, 233–245.
78A. P. Nowak, B. Wicikowska and A. Lisowska-Oleksiak, *Solid State Ion.*, 2014, **263**, 131–139.
79Y. Feng, S. Dou, Y. Wei, Y. Zhang, X. Song, X. Li and V. S. Battaglia, *ACS Omega*, 2017, **2**, 8075–8085.
80L. David, S. Bernard, C. Gervais, P. Miele and G. Singh, *J. Phys. Chem. C*, 2015, **119**, 2783–2791.
81P. E. Sanchez-Jimenez and R. Raj, *J. Am. Ceram. Soc.*, 2010, **93,** 1127-1135.
82S. H. Lee, C. Park, K. Do and H. Ahn, *Energy Stor. Mater.*, 2021, **35**, 130–141.
83M. Graczyk-Zajac, D. Vrankovic, P. Waleska, C. Hess, P. V. Sasikumar, S. Lauterbach, H.-J. Kleebe and G. D. Sorarù, *J. Mater. Chem. A*, 2018, **6**, 93–103.
84D. Ahn and R. Raj, *J. Power Sources*, 2011, **196**, 2179–2186.
85S. Nedunchezhian, R. Sujith and R. Kumar, *J. Adv. Ceram.*, 2013, **2**, 318–324.
86R. Sujith, A. B. Kousaalya and R. Kumar, *Ceram. Int.*, 2012, **38**, 1227–1233.
87J. Kaspar, M. Graczyk-Zajac and R. Riedel, *Solid State Ion.*, 2012, **225**, 527–531.
88R. A. Mantz, P. F. Jones, K. P. Chaffee, J. D. Lichtenhan, J. W. Gilman, I. M. K. Ismail and M. J. Burmeister, *Chem. Mater.*, 1996, **8**, 1250–1259.
89J. Kaspar, M. Graczyk-Zajac and R. Riedel, *J. Power Sources*, 2013, **244**, 450–455.
90V. S. Pradeep, M. Graczyk-Zajac, M. Wilamowska, R. Riedel and G. D. Soraru, *Solid State Ion.*, 2014, **262**, 22–24.
91P. Vallachira Warriam Sasikumar, E. Zera, M. Graczyk-Zajac, R. Riedel and G. D. Soraru, *J.Am. Ceram. Soc.*, 2016, **99**, 2977–2983.
92P. Wu, X. Guo, Z. Su, C. Liu, S. Chen, Z. Zheng and A. Liu, *Chem. Eng. J.*, 2022, **446**, 137354.
93M. Weinberger, C. Pfeifer, S. Schindler, T. Diemant, R. J. Behm and M. Wohlfahrt-Mehrens, *J. Mater. Chem. A*, 2015, **3**, 23707–23715.
94H. Shi, Z. Xie, Y. Zhang, A. Yuan and J. Xu, *Ionics*, 2019, **25**, 3051–3058.
95K. Xia, X. Liu, H. Liu, Y. Lu, Z. Liu, Y. Li, L. Duan, Z. Hou, R. Li and D. Wang, *Electrochim. Acta*, 2021, **372**, 137899.
96S. B. Mujib, F. Ribot, C. Gervais and G. Singh, *RSC Adv.*, 2021, **11**, 35440–35454.
97M. S. Tahir, M. Weinberger, P. Balasubramanian, T. Diemant, R. J. Behm, M. Lindén and M. Wohlfahrt-Mehrens, *J. Mater. Chem. A*, 2017, **5**, 10190–10199.
98S. B. Mujib, R. Cuccato, S. Mukherjee, G. Franchin, P. Colombo and G. Singh, *Ceram. Int.,* 2020, **46**, 3565–3573.
99Y. Xia, S. Cai, C. Lu, H. Huang, Y. Gan, J. Zhang, C. Liang, Z. Xiao and W. Zhang, *J. Alloys and Comp.*, 2020, **816**, 152595.
100J. Jang, H. Kim, H. Lim, K. jae Kim, H.-G. Jung, S.-O. Kim and W. Choi, *Chem. Eng. J.*, 2020, **401**, 126091.
101J. Gangadhar, A. Maheshwari, R. K. Bordia, C. N. Shyam Kumar, C. Kubel and R. Sujith, *Ceram, Int.*, 2020, **46**, 28156–28164.
102Z. Wu, X. Cheng, D. Tian, T. Gao, W. He and C. Yang, *Chem. Eng. J..,* 2019, **375**, 121997.
103D. Knozowski, M. Graczyk-Zajac, G. Trykowski and M. Wilamowska-Zawłocka, *Mater.*, 2020, **13**, 4302.
104D. Knozowski, M. Graczyk-Zając, D. Vrankovic, G. Trykowski, M. Sawczak, D. M. De Carolis and M. Wilamowska-Zawłocka, *Comp. Part B: Eng.*, 2021, **225**, 109302.
105I. Saleh and R. Raj, *J. Power Sources*, 2016, **310**, 18–25.
106J. Shen, D. Ahn and R. Raj, *J.Power Sources*, 2011, **196**, 2875–2878.

107R. Bhandavat and G. Singh, *J. Phys. Chem. C*, 2013, **117**, 11899–11905.
108H. Li, X. Yan, Z. Ma, Y. Zhang, C. Li, W. Xiao and Y. Jiang, *Ceram. Int.*, 2021, **47**, 6867–6874.
109Y. Li, Y. Hu, Y. Lu, S. Zhang, G. Xu, K. Fu, S. Li, C. Chen, L. Zhou, X. Xia and X. Zhang, *J. Power Sources*, 2014, **254**, 33–38.
110M. Ma, H. Wang, X. Li, K. Peng, L. Xiong and X. Du, *J. Eur. Ceram. Soc.*, 2020, **40**, 5238–5246.
111L. David, K. M. Shareef, M. A. Abass and G. Singh, *RSC Adv.*, 2016, **6**, 53894–53902.
112M. S. Kolathodi, L. David, M. A. Abass and G. Singh, *RSC Adv.*, 2016, **6**, 74323–74331.
113M. Ma, H. Wang, L. Xiong, S. Huang, X. Li and X. Du, *Carbon*, 2022, **186**, 273–281.
114Y. Ren, B. Yang, X. Huang, F. Chu, J. Qiu and J. Ding, *Solid State Ion.*, 2015, **278**, 198–202.
115F. Ji, Y.-L. Li, J.-M. Feng, D. Su, Y.-Y. Wen, Y. Feng and F. Hou, *J. Mater. Chem.*, 2009, **19**, 9063.
116Z. Sang, X. Yan, L. Wen, D. Su, Z. Zhao, Y. Liu, H. Ji, J. Liang and S. X. Dou, *Energy Stor.Mater.*, 2020, **25**, 876–884.
117Z. Sang, Z. Zhao, D. Su, P. Miao, F. Zhang, H. Ji and X. Yan, *J. Mater. Chem. A*, 2018, **6**, 9064–9073.
118G. Shao, D. A. H. Hanaor, J. Wang, D. Kober, S. Li, X. Wang, X. Shen, M. F. Bekheet and A. Gurlo, *ACS Appl. Mater. Interfaces*, 2020, **12**, 46045–46056.
119Z. Zhang, J. E. Calderon, S. Fahad, L. Ju, D.-X. Antony, Y. Yang, A. Kushima and L. Zhai, *ACS Appl. Mater. Interfaces*, 2021, **13**, 9794–9803.
120Md. S. Islam, M. R. Karim, S. Islam, J. Kim, N. N. Rabin, R. Ohtani, M. Nakamura, M. Koinuma and S. Hayami, *Chem. Select*, 2016, **1**, 6429–6433.
121L. David, R. Bhandavat, U. Barrera and G. Singh, *Nat Commun*, 2016, **7**, 10998.
122H. Hong, W. Liu, M. Zhang, Y. Wang and Y. Chen, *J. Alloys Compd.*, 2021, **857**, 157476.
123R. J. -C. Dubey, P. V. W. Sasikumar, F. Krumeich, G. Blugan, J. Kuebler, K. V. Kravchyk, T. Graule and M. V. Kovalenko, *Adv. Sci.*, 2019, **6**, 1901220.
124K. D, V. W. S. P, M. P, B. G, G. M, K. N and W.-Z. M, *Nanomater. (Basel, Switzerland)*, , DOI:10.3390/nano12030410.
125J. Rohrer, D. Vrankovic, D. Cupid, R. Riedel, H. J. Seifert, K. Albe and M. Graczyk-Zajac, *Int. J. Mater. Res.*, 2017, **108**, 920–932.
126A. Tolosa, M. Widmaier, B. Krüner, J. M. Griffin and V. Presser, *Sustain. Energy Fuels*, 2017, **2**, 215–228.
127R. J.-C. Dubey, P. V. W. Sasikumar, N. Cerboni, M. Aebli, F. Krumeich, G. Blugan, K. V. Kravchyk, T. Graule and M. V. Kovalenko, *Nanoscale*, 2020, **12**, 13540–13547.
128D. Kim, H. Kim, H. Lim, K. J. Kim, H.-G. Jung, D. Byun, C. Kim and W. Choi, *Int. J. Energy Res.*, 2020, **44**, 11473–11486.
129S. Dey, S. B. Mujib and G. Singh, *Nanomater. (Basel)*, 2022, **12**, 553.
130J. Kaspar, M. Graczyk-Zajac, S. Lauterbach, H.-J. Kleebe and R. Riedel, *J. Power Sources*, 2014, **269**, 164–172.
131X. Liu, K. Xie, J. Wang, C. Zheng and Y. Pan, *J. Mater. Chem.*, 2012, **22**, 19621–19624.
132S. Choi, D. S. Jung and J. W. Choi, *Nano Lett.*, 2014, **14**, 7120–7125.
133D. Vrankovic, M. Graczyk-Zajac, C. Kalcher, J. Rohrer, M. Becker, C. Stabler, G. Trykowski, K. Albe and R. Riedel, *ACS Nano*, 2017, **11**, 11409–11416.
134D. Vrankovic, K. Wissel, M. Graczyk-Zajac and R. Riedel, *Solid State Ion.*, 2017, **302**, 66–71.
135A Nanostructured Si/SiOC Composite Anode with Volume-Change-Buffering Microstructure for Lithium-Ion Batteries - Wu - 2019 - Chemistry – A European

Journal - Wiley Online Library, https://chemistry-europe.onlinelibrary.wiley.com/doi/full/10.1002/chem.201805255, (accessed October 18, 2022).
136W. Wei, K. Xu, N. Liao and W. Xue, *Appl. Mater. Today*, 2020, **20**, 100773.
137J. Kaspar, C. Terzioglu, E. Ionescu, M. Graczyk-Zajac, S. Hapis, H.-J. Kleebe and R. Riedel, *Adv. Funct. Mater.*, 2014, 8.
138C. Shi, H. Huang, Y. Xia, J. Yu, R. Fang, C. Liang, J. Zhang, Y. Gan and W. Zhang, *Chem. Eur. J.*, 2019, **25**, 7719–7725.
139K. Xia, L. Qu, X. Liu, H. Han, Z. Hou, Y. Li and S. Deng, *Appl. Surf. Sci.*, 2020, **506**, 144775.
140S. Eun Wang, J.-S. Park, M. Ji Kim, Y. Chan Kang and D. Soo Jung, *Appl. Surf. Sci.*, 2022, **589**, 152952.
141M. A. Abass, A. A. Syed, C. Gervais and G. Singh, *RSC Adv.*, 2017, **7**, 21576–21584.
142H. Huang, C. Shi, R. Fang, Y. Xia, C. Liang, Y. Gan, J. Zhang, X. Tao and W. Zhang, *Chem. Eng. J..*, 2019, **359**, 584–593.

143G. Zhu, R. Guo, W. Luo, H. K. Liu, W. Jiang, S. X. Dou and J. Yang, *Natl. Sci. Rev.*, 2021, **8**, nwaa152.

144J. Shen and R. Raj, *J. Power Sources*, 2011, **196**, 5945–5950.
145B. Krüner, C. Odenwald, A. Tolosa, A. Schreiber, M. Aslan, G. Kickelbick and V. Presser, *Sustain. Energy Fuels*, 2017, **1**, 1588–1600.
146H. T. T. Le, D. T. Ngo, X.-M. Pham, T.-Y. Nguyen, T.-D. Dang and C.-J. Park, *J. Power Sources*, 2019, **440**, 227104.
147Q. Meng, G. Li, J. Yue, Q. Xu, Y.-X. Yin and Y.-G. Guo, *ACS Appl. Mater. Interfaces*, 2019, **11**, 32062–32068.
148L. Jin, C. Shen, A. Shellikeri, Q. Wu, J. Zheng, P. Andrei, J.-G. Zhang and J. P. Zheng, *Energy Environ. Sci.*, 2020, **13**, 2341–2362.
149Y. Xia, R. Fang, Z. Xiao, L. Ruan, R. Yan, H. Huang, C. Liang, Y. Gan, J. Zhang, X. Tao and W. Zhang, *RSC Adv.*, 2016, **6**, 69764–69772.
150P. Tao, J. He, T. Shen, Y. Hao, J. Yan, Z. Huang, X. Xu, M. Li and Y. Chen, *Adv. Mater. Interfaces*, 2019, **6**, 1900460.
151J. Wang, C. Luo, T. Gao, A. Langrock, A. C. Mignerey and C. Wang, *Small*, 2015, **11**, 473–481.
152D. M. Soares and G. Singh, *Nanotechnol.*, 2020, **31**, 145403.
153H. Lim, S. Yu, W. Choi and S.-O. Kim, *ACS Nano*, 2021, **15**, 7409–7420.
154Y. Lee, K. Y. Lee and W. Choi, *Adv. Funct. Mater.*, 2017, **27**, 1702607.
155C. Chandra and J. Kim, *Chem. Eng. J.*, 2018, **338**, 126–136.
156C. Chandra, W. Devina, S. Alvin and J. Kim, *Chem. Eng. J..,* 2021, **404**, 126520.
157X. Dou, D. Buchholz, M. Weinberger, T. Diemant, M. Kaus, S. Indris, R. J. Behm, M. Wohlfahrt-Mehrens and S. Passerini, *Small Methods*, 2019, **3**, 1800177.
158C. Chandra, H. S. Cahyadi, S. Alvin, W. Devina, J.-H. Park, W. Chang, K. Y. Chung, S. K. Kwak and J. Kim, *Chem. Mater.*, 2020, **32**, 410–423.
159J. Kaspar, M. Storch, C. Schitco, R. Riedel and M. Graczyk-Zajac, *J. Electrochem. Soc.*, 2015, **163**, A156.
160R. N. Putra, M. Halim, G. Ali, S. F. Shaikh, A. M. Al-Enizi, T. Fazal, F. J. Iftikhar and A. N. S. Saqib, *New J. Chem.*, 2020, **44**, 14035–14040.
161H. Cheng, N. Garcia-Araez and A. L. Hector, *Mater. Adv.*, 2021, **2**, 7956–7966.
162J. Pan, W. Zhong, Z. Gao, X. Yang, Y. Zhang, Y. Guan and X. Yan, *Ceram. Intern.*, 2021, **47**, 27833–27842.

163M. Halim, G. Liu, R. E. A. Ardhi, C. Hudaya, O. Wijaya, S.-H. Lee, A.-Y. Kim and J. K. Lee, *ACS Appl. Mater. Interfaces*, 2017, **9**, 20566–20576.

164A. Meier, M. Weinberger, K. Pinkert, M. Oschatz, S. Paasch, L. Giebeler, H. Althues, E. Brunner, J. Eckert and S. Kaskel, *Micro. Mesopor. Mater.,* 2014, **188**, 140–148.

165L. Duan, Q. Ma, L. Mei and Z. Chen, *Micropor. Mesopor. Mater.*, 2015, **202**, 97–105.

166A. Tolosa, B. Krüner, N. Jäckel, M. Aslan, C. Vakifahmetoglu and V. Presser, *J Power Sources*, 2016, **313**, 178–188.

167P. Pazhamalai, K. Krishnamoorthy, S. Sahoo, V. K. Mariappan and S.-J. Kim, *Chem. Eng. J.*, 2020, **387**, 123886.

168U. Okoroanyanwu, A. Bhardwaj, V. Einck, A. Ribbe, W. Hu, J. M. Rodriguez, W. R. Schmidt and J. J. Watkins, *Chem. Mater.*, 2021, **33**, 678–694.

169I. P. Swain and S. K. Behera, *Ceram. Intern.*, 2022, **48**, 8216–8227.

170M. A. Mazo, M. T. Colomer, A. Tamayo and J. Rubio, *Micropor. Mesopor. Mater.*, 2022, **330**, 111604.

171G. Jella, D. K. Panda, N. Sapkota, M. Greenough, S. P. Datta, A. M. Rao, R. Sujith and R. K. Bordia, *ACS Appl. Mater. Interfaces.*, 2023, **15**, 30039-30051.